Intermolecular torsional motion of a π-aggregated dimer probed by two-dimensional electronic spectroscopy

Joachim Seibt and Alexander Eisfeld

Citation: J. Chem. Phys. **136**, 024109 (2012); doi: 10.1063/1.3674993
View online: http://dx.doi.org/10.1063/1.3674993
View Table of Contents: http://jcp.aip.org/resource/1/JCPSA6/v136/i2
Published by the American Institute of Physics.

Intermolecular torsional motion of a π-aggregated dimer probed by two-dimensional electronic spectroscopy

Joachim Seibt[1] and Alexander Eisfeld[1,2,a)]
[1]*Max Planck Institute for the Physics of Complex Systems, Nöthnitzer Strasse 38, 01187 Dresden, Germany*
[2]*Department of Chemistry and Chemical Biology, Harvard University, 12 Oxford Street, Cambridge, Massachusetts 02138, USA*

(Received 4 November 2011; accepted 14 December 2011; published online 13 January 2012)

The energetic splitting of the two exciton states of a molecular dimer depends strongly on the relative orientation of the monomers with respect to each other. The curvature of the corresponding adiabatic potential energy surfaces can lead to torsional motion of the monomers. It has been suggested recently that this torsional motion could provide a possible relaxation mechanism for the upper state which proceeds via a crossing of the two singly excited state potentials. Another, competing, relaxation mechanism is provided by coupling to the environment, leading to direct exciton relaxation. Here we examine theoretically the combined dynamics of torsional motion and excitonic relaxation for a π-aggregated dimer. Using two-dimensional (2D) spectroscopy, it is shown how torsional motion through a crossing of the adiabatic excitonic potential surfaces could be distinguished from direct relaxation. For the calculations a mixed quantum/classical approach is used, where the torsional motion is treated by an Ehrenfest type of equation, while the excitonic dynamics including dephasing and direct relaxation is described by a quantum master equation. © *2012 American Institute of Physics*. [doi:10.1063/1.3674993]

I. INTRODUCTION

The study of the optical properties of molecular dimers plays an important role in understanding excitonic couplings in molecular aggregates, since one can perform detailed investigations including nuclear degrees of freedom (see, e.g., Refs. 1–11). In such molecular dimers, transition dipole-dipole interaction leads to a splitting of the two singly excited states.[12] The absorption strength of each state depends strongly on the relative orientation of the monomers. For example, if both transition dipoles are parallel to each other and perpendicular to the distance vector between the monomers, only absorption into the energetically higher dimer state is allowed.[13] If the monomers are not perfectly parallel, both states carry oscillator strength.

Usually it is assumed that the arrangement of the monomers in the dimer is time-independent. However, recent quantum chemical investigations of dimers formed by perylene bisimid molecules[14,15] suggest that upon excitation from the electronic ground state to the excited states of the dimer a strong torsional motion takes place, due to the curvature of the respective excited state potential surfaces (as sketched in Fig. 1(c)). It has been suggested that this torsional motion plays an important role in the relaxation dynamics. Quantum chemical calculations[14] indicate that the electronic potential curves of the two exciton states cross each other and it has been proposed that the torsional motion takes place through the crossing. Recently also the involvement of charge transfer states has been discussed.[15]

On the other hand, interaction with the environment also provides an efficient relaxation channel. One expects that in solution the large coupling strength of the excited states to the environment results in fast relaxation on a timescale shorter than the time needed to reach the crossing region (picosecond range). Thus the torsional dynamics would play a minor role. However, for the case with weak coupling to the environment the relaxation associated with torsional motion might become the dominant channel. Such a situation can for example realized experimentally in Helium nanodroplets.[10]

In the present work, we aim at a distinction between relaxation processes induced by the environment and torsional motion through the crossing by means of two-dimensional (2D) electronic spectroscopy. Two-dimensional electronic spectroscopy has proven to be an informative tool that gives insight into the dynamics of molecular systems.[16,17]

Two-dimensional electronic spectroscopy yields information on the exciton dynamics in molecular aggregates[18] and was used to obtain information about coherence and transfer properties of various systems. In particular the application to biological light harvesting complexes has become a matter of increasing interest in the recent years.[19–24] Two-dimensional electronic spectroscopy has for example also been used to study the delocalization length[25] and interactions[26] in molecular J-aggregates. Since the dimer is the smallest aggregate (and allows a fairly detailed theoretical treatment) it has been extensively investigated.[27–34] In these studies, the position and the orientation of the molecules within the aggregates is assumed to be time-independent.

The paper is organized as follows: In Sec. I we introduce the employed dimer model system together with a specification of the chosen potentials with respect to the torsional degree of freedom. An estimate of the timescale related to the torsional dynamics is given. In Secs. III and IV the general expressions used to calculate the 2D signals on the basis of response functions are introduced. In Sec. VI we show model

a)Electronic mail: eisfeld@mpipks-dresden.mpg.de.

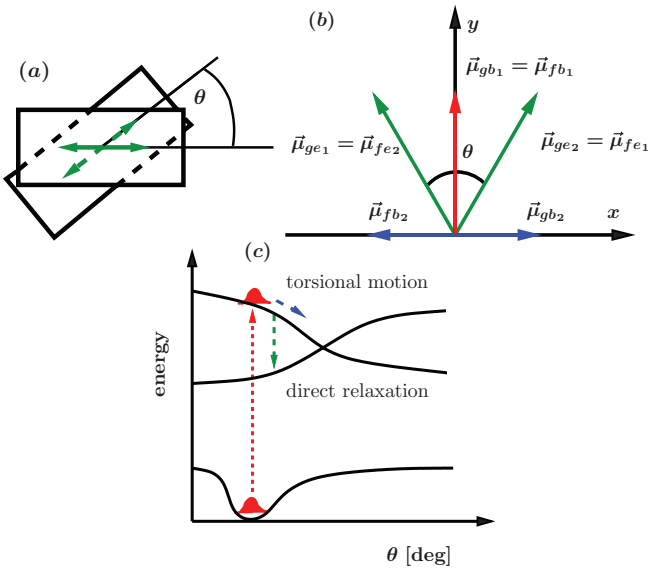

FIG. 1. (a) Sketch of the arrangement of the two monomer units, which can rotate around the stack axis of the dimer. The corresponding angle is denoted by θ and defined as shown in the figure. (b) Sketch of the coplanar transition dipole moments within the (x, y)-plane of the body frame. (c) Sketch of the potential energy surfaces with an illustration of torsional motion and direct relaxation.

calculations that elucidate the signatures of the relaxation and torsional motion. A formulation of the response functions in rotating wave approximation is given in Appendix A. In Appendix B we briefly discuss orientational averaging, which is important for randomly oriented dimers. In Appendix C the double coherence (DC) contribution is given.

II. MODEL OF THE MOLECULAR DIMER

For each monomer we take the electronic ground state $|\phi_n^{\mathbf{g}}\rangle$ and the singly excited state $|\phi_n^{\mathbf{e}}\rangle$ into account ($n = 1, 2$). As an electronic basis for the dimer we define the states

$$|\mathbf{g}\rangle = |\phi_1^{\mathbf{g}}\rangle|\phi_2^{\mathbf{g}}\rangle, \tag{1}$$

$$|\mathbf{e_1}\rangle = |\phi_1^{\mathbf{e}}\rangle|\phi_2^{\mathbf{g}}\rangle, \tag{2}$$

$$|\mathbf{e_2}\rangle = |\phi_1^{\mathbf{g}}\rangle|\phi_2^{\mathbf{e}}\rangle, \tag{3}$$

$$|\mathbf{f}\rangle = |\phi_1^{\mathbf{e}}\rangle|\phi_2^{\mathbf{e}}\rangle. \tag{4}$$

We will refer to the state $|\mathbf{g}\rangle$ as the dimer electronic ground state. The states $|\mathbf{e_1}\rangle$ and $|\mathbf{e_2}\rangle$ span the so-called one exciton space. Finally the state $|\mathbf{f}\rangle$ will be referred to as the doubly excited state.

As mentioned in the introduction we are interested in the dynamics of the relative orientation of the two monomers with respect to each other, which is induced by a change of the electronic states. In the following we will only take one degree of freedom for the relative motion of the monomers into account, which corresponds to a torsion as sketched in Fig. 1. This coordinate is denoted by θ.

The dimer Hamiltonian can be expanded in the electronic basis given by Eqs. (1)–(4). It reads

$$\begin{aligned} H_D = {} & |\mathbf{g}\rangle \left(H_1^{\mathbf{g}} + H_2^{\mathbf{g}}\right) \langle \mathbf{g}| \\ & + |\mathbf{e_1}\rangle \left(H_1^{\mathbf{e}} + H_2^{\mathbf{g}}\right) \langle \mathbf{e_1}| + |\mathbf{e_1}\rangle J \langle \mathbf{e_2}| \\ & + |\mathbf{e_2}\rangle J \langle \mathbf{e_1}| + |\mathbf{e_2}\rangle \left(H_1^{\mathbf{g}} + H_2^{\mathbf{e}}\right) \langle \mathbf{e_2}| \\ & + |\mathbf{f}\rangle \left(H_1^{\mathbf{e}} + H_2^{\mathbf{e}}\right) \langle \mathbf{f}|, \end{aligned} \tag{5}$$

where the Hamiltonians $H_i^{\mathbf{g}}$ and $H_i^{\mathbf{e}}$ are related to the ground- and singly excited state of monomer unit n and J is the transition dipole-dipole interaction between the monomers. This interaction has a strong dependence on the relative orientation of the monomers with respect to each other.

To proceed further, we will use the fact that the electronic transition energy of the monomers is of the order of 2–3 eV, which is roughly ten times larger than the interaction between the monomers. In zeroth order the dominant interaction between the monomers will be a resonant dipole-dipole interaction J between the states $|\mathbf{e_1}\rangle$ and $|\mathbf{e_2}\rangle$ (in the disorder-free case degenerate), which leads to a splitting in the one-exciton space. We assume that in the ground state $|\mathbf{g}\rangle$ and in the doubly excited state $|\mathbf{f}\rangle$ the interaction only leads to an energy shift. Note that this shift and the interaction J depend on the angle θ.

If we ignore static disorder and take the transition energies of the two monomers to be equal, the states

$$|\mathbf{b_{1,2}}\rangle \equiv \frac{1}{\sqrt{2}}(|\mathbf{e_2}\rangle \pm |\mathbf{e_1}\rangle) \tag{6}$$

are obtained from the diagonalization of the one exciton space, where in the localized state representation coupling matrix elements appear.

In Born-Oppenheimer approximation, the dimer Hamiltonian can then be written as

$$H_D(\theta) = \sum_{j\in\{\mathbf{g},\mathbf{b_1},\mathbf{b_2},\mathbf{f}\}} H_j(\theta). \tag{7}$$

Here the Hamiltonians for nuclear motion in the electronic state j are given by

$$H_j(\theta) \equiv T + V_j(\theta), \tag{8}$$

where T denotes the kinetic energy operator of the torsional motion and $V_j(\theta)$ is the Born-Oppenheimer surface of state $j = \mathbf{g}, \mathbf{b_1}, \mathbf{b_2}, \mathbf{f}$. In Sec. II A the Born-Oppenheimer potentials are specified.

For the calculation of optical spectra the transition dipoles of the dimer are of primary importance. In Fig. 1 the transition dipoles of the dimer are sketched. We chose the body-frame coordinate system $(\hat{x}, \hat{y}, \hat{z})$ such that the z-axis is perpendicular to the plane spanned by the monomer transition dipoles $\vec{\mu}_1^{\mathbf{ge}}$ and $\vec{\mu}_2^{\mathbf{ge}}$. The y-axis is the bisecting line between $\vec{\mu}_1^{\mathbf{ge}}$ and $\vec{\mu}_2^{\mathbf{ge}}$. Here $\vec{\mu}_n^{\mathbf{ge}} \equiv \langle \phi_n^{\mathbf{g}} | \vec{\mu}_n | \phi_n^{\mathbf{e}} \rangle$ with $\vec{\mu}_n$ denoting the dipole operator of monomer n.

In this body-fixed coordinate system one has

$$\vec{\mu}_1^{\mathbf{ge}}(\theta) = \mu_1(\hat{y}\,\cos(\theta/2) - \hat{x}\,\sin(\theta/2)), \tag{9}$$

$$\vec{\mu}_2^{\mathbf{ge}}(\theta) = \mu_2(\hat{y}\,\cos(\theta/2) + \hat{x}\,\sin(\theta/2)), \tag{10}$$

where μ_n denotes the absolute value of $\vec{\mu}_n^{\mathbf{ge}}$. In the following, we take the absolute values of the monomer transition dipoles to be equal, i.e., $\mu_1 = \mu_2 \equiv \mu$. The transition dipole operator of the dimer is given by $\hat{\mu} = \hat{\mu}_1 + \hat{\mu}_2$. In the body-fixed frame of the dimer one thus has

$$\vec{\mu}_I \equiv \vec{\mu}_{\mathbf{gb_1}} = \sqrt{2}\mu\cos(\theta/2)\hat{y}, \tag{11}$$

$$\vec{\mu}_{II} \equiv \vec{\mu}_{\mathbf{gb_2}} = \sqrt{2}\mu \sin(\theta/2)\hat{x}. \tag{12}$$

Note the strong dependence on the transition dipole moments on the torsional angle θ. Similarly, for the transition from the singly excited manifold to the doubly excited state one has

$$\vec{\mu}_{III} \equiv \vec{\mu}_{\mathbf{b_1 f}} = \vec{\mu}_{\mathbf{gb_1}} = \vec{\mu}_{I}, \tag{13}$$

$$\vec{\mu}_{IV} \equiv \vec{\mu}_{\mathbf{b_2 f}} = -\vec{\mu}_{\mathbf{gb_2}} = -\vec{\mu}_{II}. \tag{14}$$

There are no direct transitions between $|\mathbf{g}\rangle$ and $|\mathbf{f}\rangle$. This assumption is justified by the rotating wave approximation, as the chosen pulse frequency distributions yield no appreciable contribution, where the resonance condition with the respective energy difference is fulfilled. An illustration of the transition dipole moments within the (x, y)-plane is shown in Fig. 1.

A. The potential energy surfaces

In the following, we will investigate how different system dynamics, either relaxation induced by system-bath interaction or torsional motion through the curve crossing (CC), influence the 2D-specta. For this aim we do not use the complicated potential obtained from quantum chemical calculations,[14] but rather simple forms of these potentials, which however share the characteristic properties of the quantum chemical results. The potentials are chosen such that the features of torsional motion become clearly visible.

The used model potentials are shown in Fig. 2. The ground state potential has a minimum at roughly 30° and the two exciton states cross each other at around 60°.

In the singly excited state the potentials are chosen in a way that the gradient of the energetically higher 1-exciton state potential at the absorption point leads to torsional motion up to the intersection with the energetically lower 1-exciton state potential within the range of picoseconds. In the present work, we will focus on the signatures of this dynamics in the 2D spectra. To understand the calculated 2D spectra more easily, we will take the potential surface of the doubly excited state, which also plays a role in nonlinear spectroscopy, to be independent of θ. The treatment of more complicated potential surfaces is straightforward.

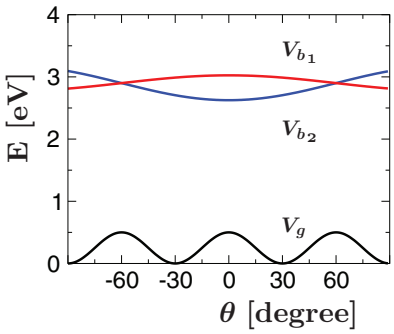

FIG. 2. Illustration of the potentials used for the calculations. The doubly excited surface (not shown) is taken to be independent of the torsional angle θ.

B. Estimate of time scales

Before considering the calculation of 2D spectra in detail, we will estimate the timescale for torsional dynamics. The time T^* needed for the motion in the upper state from the absorption point to the curve crossing at an angle of $\theta^* = 60^\circ$ can be obtained from the solution of Newton's equation of motion $I\frac{d^2}{dt^2}\theta = -\frac{dV_{\mathbf{b_1}}}{d\theta}$, where I denotes the moment of inertia. For the calculations, the value $I = 2.7 \times 10^{-43}\,\mathrm{kg\,m^2}$ is used.[49] As a plausibility test, we also determined the moment of inertia of a perylene bisimid molecule from the molecular geometry and found $I \sim 1.063 \times 10^{-43}\,\mathrm{kg\,m^2}$. From these values we estimate the time T^* to be of the order of a few ps.

III. CALCULATION OF 2D-SPECTRA

Two-dimensional optical spectra originate from the interaction of three laser pulses with a material system. We define the components of all electric fields with respect to a laboratory system $\hat{X}, \hat{Y}, \hat{Z}$. The dimers will be assumed to be randomly oriented within this laboratory system. By interaction with the electric fields the third order nonlinear polarization $\vec{P}^{(3)}(t)$ is generated. The jth electric field $\vec{E}_j(\vec{r}, t')$ at time t' and position $\vec{r}$ is

$$\begin{aligned}\vec{E}_j(\vec{r}, t') &= \hat{\epsilon}_j\, E_j(t' - t_j)\cos(\omega_j(t' - t_j) - \vec{k}_j\vec{r}) \\ &= \frac{1}{2}\hat{\epsilon}_j\, E_j(t' - t_j)\, \mathrm{e}^{-i(\omega_j(t'-t_j)-\vec{k}_j\vec{r})} + \mathrm{c.c.}\end{aligned} \tag{15}$$

Here $\vec{k}_j$ denotes the wave-vector, ω_j is the frequency, and $\hat{\epsilon}_j$ denotes the polarization of the jth field. The envelope functions $E_j(t - t_j)$ of the pulses are localized around the times t_j. The total electric field is then given by

$$\vec{E}(\vec{r}, t') = \sum_{j=1}^{3} \vec{E}_j(\vec{r}, t'). \tag{16}$$

The outgoing field is detected in a phase-matching direction, which we choose as $\vec{k}_s = -\vec{k}_1 + \vec{k}_2 + \vec{k}_3$.

The third-order polarization $P^{(3)}_{\alpha\beta\gamma\delta}(\vec{r}, t')$ for finite pulse widths is obtained from a convolution of the third order response function $S^{(3)}_{\alpha\beta\gamma\delta}$ with the pulses:

$$\begin{aligned}P^{(3)}_{\alpha\beta\gamma\delta}(\vec{r}, t') = \int_0^\infty d\tau_3 \int_0^\infty d\tau_2 \int_0^\infty d\tau_1 S^{(3)}_{\alpha\beta\gamma\delta}(\tau_3, \tau_2, \tau_1) \\ \times E_\beta(\vec{r}, t' - \tau_3) E_\gamma(\vec{r}, t' - \tau_3 - \tau_2) \\ \times E_\delta(\vec{r}, t' - \tau_3 - \tau_2 - \tau_1).\end{aligned} \tag{17}$$

In this work we use the Greek indices α, β, γ, δ, which also appear in Eq. (17), to denote the projection onto the axes $\{\hat{\alpha}, \hat{\beta}, \hat{\gamma}, \hat{\delta}\} \in \{\hat{X}, \hat{Y}, \hat{Z}\}$ of the laboratory frame. For example, $\mu_\alpha = \hat{\alpha} \cdot \hat{\mu}(t)$ is the projection of the dipole-operator of the dimer onto the lab-axis $\hat{\alpha}$. The time intervals of free propagation are defined as $\tau_k = t'_{k+1} - t'_k$, where t'_k denotes the time at which the kth interaction of the system with the electric field is evaluated. The indices are related to the temporal sequence of the interactions, so that τ_k is always positive. For the characterization of pulse sequences in third order nonlinear spectroscopy it is convenient to introduce characteristic time intervals. While the coherence time τ

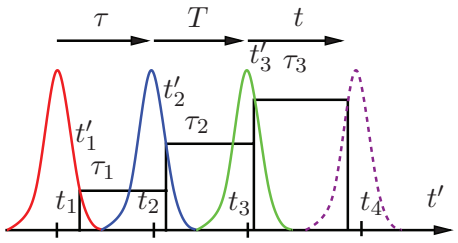

FIG. 3. Sketch of the pulse sequence, where the time variables and intervals used in the present work are indicated.

$= t_2 - t_1$ switches sign upon exchange of the time ordering of pulse 1 and pulse 2, the population time $T = t_3 - max(t_1, t_2)$ is related to the delay between pulse 3 and the second incoming pulse (either pulse 1 or pulse 2), see Fig. 3 and Ref. 35. The detection time t starts at the arrival of the third pulse and measures the interval up to the detection of the signal.

The 2D-spectrum is obtained by the two-dimensional Fourier-transform[28]

$$\sigma_{\alpha\beta\gamma\delta}(\omega_\tau, T, \omega_t) = i \int_{-\infty}^{\infty} d\tau \int_{-\infty}^{\infty} dt e^{-i\omega_\tau \tau} \times e^{i\omega_t t} P^{(3)}_{\alpha\beta\gamma\delta}(\tau, T, t), \quad (18)$$

where the third order polarization $P^{(3)}_\alpha(t', \vec{r})$ from Eq. (17) is expressed as a function of τ, T, and t. The position vector is not included anymore, since for the given detection direction only the components with a phase factor $\exp(i(-\vec{k}_1 + \vec{k}_2 + \vec{k}_3)\vec{r})$ are retained. Thus, a separation of this factor is possible. Depending on whether the polarization evolves with a positive or negative complex phase during τ, rephasing and non-rephasing signal contributions are distinguished (see Appendix A).

IV. EVALUATION OF THE RESPONSE FUNCTIONS

The third order response function, which is used to calculate $P^{(3)}_\alpha(t', \vec{r})$, is a fourth rank tensor, given by

$$S^{(3)}_{\alpha\beta\gamma\delta}(\tau_3, \tau_2, \tau_1) = \langle \tilde{S}^{(3)}_{\alpha\beta\gamma\delta} \rangle \quad (19)$$

Here $\langle \cdots \rangle$ denotes an average over all orientations of the dimers (discussed in detail in Appendix B) and

$$\tilde{S}^{(3)}_{\alpha\beta\gamma\delta}(\tau_3, \tau_2, \tau_1) = \left(\frac{i}{\hbar}\right)^3 \langle\langle \mu_\alpha | \mathcal{G}(\tau_3) \mathcal{V}_\beta \mathcal{G}(\tau_2) \mathcal{V}_\gamma \mathcal{G}(\tau_1) \mathcal{V}_\delta | \rho_0 \rangle\rangle. \quad (20)$$

Here $\langle\langle A|B\rangle\rangle \equiv \mathrm{Tr}_{\mathrm{el}}\{A^\dagger B\}$ and $\mathcal{V}$ denotes the transition operators in Liouville space with matrix elements given by

$$\langle\langle kl \left| \mathcal{V}_\beta(\theta) \right| mn \rangle\rangle = \delta_{ln}(\vec{\mu}_{km}(\theta))_\beta - \delta_{km}(\vec{\mu}_{ln}(\theta))_\beta, \quad (21)$$

where the indices k, l, m, n label the eigenstates of the dimer. We denote by $(\vec{\mu}_{ln})_\beta$ the component of the transition dipole operator for a transition from electronic eigenstate l to n along the $\hat{\beta}$-axis of the laboratory frame. The Green-operators in Liouville space are given by

$$\mathcal{G}(t') = \Theta(t') \exp(-i\hat{\mathcal{L}}t'/\hbar), \quad (22)$$

where the Liouville operator $\hat{\mathcal{L}}$ is defined by $\hat{\mathcal{L}}\rho = [H_D, \rho] - \Gamma\rho$. The operator Γ has been introduced to account for dissipative processes. The initial state will in the following be taken to be of the form

$$\rho_0 = |\mathbf{g}\rangle\langle\mathbf{g}| \otimes \rho^{\mathrm{ini}}_{\mathrm{nuc}}. \quad (23)$$

Thereby $\rho^{\mathrm{ini}}_{\mathrm{nuc}}$ is related to the initial position of the torsional coordinate at the minimum of the ground state.

It is convenient to write

$$\tilde{S}^{(3)}_{\alpha\beta\gamma\delta}(\tau_3, \tau_2, \tau_1) = \left(\frac{i}{\hbar}\right) \sum_{n=1}^{4} \left[(\tilde{R}_n)_{\alpha\beta\gamma\delta}(\tau_3, \tau_2, \tau_1) - (\tilde{R}_n)^*_{\alpha\beta\gamma\delta}(\tau_3, \tau_2, \tau_1) \right], \quad (24)$$

where the response functions $(\tilde{R}_n)_{\alpha\beta\gamma\delta}$ are given by

$$(\tilde{R}_1)_{\alpha\beta\gamma\delta}(\tau_1, \tau_2, \tau_3) = \sum \mathrm{Tr}_{\mathrm{nuc}}\{(\vec{\mu}_{nm})_\alpha \mathcal{G}_{mn,il}(\tau_3)(\vec{\mu}_{lj})_\beta \times \mathcal{G}_{ij,eh}(\tau_2)(\vec{\mu}_{hf})_\gamma \mathcal{G}_{ef,ca}(\tau_1)(\vec{\mu}_{ca})_\delta \times P(a)\rho^{\mathrm{ini}}_{\mathrm{nuc}}\}, \quad (25)$$

$$(\tilde{R}_2)_{\alpha\beta\gamma\delta}(\tau_1, \tau_2, \tau_3) = \sum \mathrm{Tr}_{\mathrm{nuc}}\{(\vec{\mu}_{nm})_\alpha \mathcal{G}_{mn,il}(\tau_3)(\vec{\mu}_{lj})_\beta \times \mathcal{G}_{ij,gf}(\tau_2)(\vec{\mu}_{ge})_\gamma \mathcal{G}_{ef,ad}(\tau_1)(\vec{\mu}_{da})_\delta \times P(a)\rho^{\mathrm{ini}}_{\mathrm{nuc}}\}, \quad (26)$$

$$(\tilde{R}_3)_{\alpha\beta\gamma\delta}(\tau_1, \tau_2, \tau_3) = \sum \mathrm{Tr}_{\mathrm{nuc}}\{(\vec{\mu}_{nm})_\alpha \mathcal{G}_{mn,kj}(\tau_3)(\vec{\mu}_{ki})_\beta \times \mathcal{G}_{ij,eh}(\tau_2)(\vec{\mu}_{hf})_\gamma \mathcal{G}_{ef,ad}(\tau_1)(\vec{\mu}_{da})_\delta \times P(a)\rho^{\mathrm{ini}}_{\mathrm{nuc}}\}, \quad (27)$$

$$(\tilde{R}_4)_{\alpha\beta\gamma\delta}(\tau_1, \tau_2, \tau_3) = \sum \mathrm{Tr}_{\mathrm{nuc}}\{(\vec{\mu}_{nm})_\alpha \mathcal{G}_{mn,kj}(\tau_3)(\vec{\mu}_{ki})_\beta \times \mathcal{G}_{ij,gf}(\tau_2)(\vec{\mu}_{ge})_\gamma \mathcal{G}_{ef,ca}(\tau_1)(\vec{\mu}_{ca})_\delta \times P(a)\rho^{\mathrm{ini}}_{\mathrm{nuc}}\}. \quad (28)$$

Here the sum runs over all Latin indices which label the four electronic states of the dimer.

Note that we have expanded only with respect to electronic degrees of freedom. All dipole matrix elements and all Green-operators are still operators with respect to the torsional angle.

The green operators $\mathcal{G}$ appearing in Eqs. (25)–(28) can be obtained from a solution of the Liouville-von-Neumann equation, which we take to be of the form ($\hbar = 1$)

$$\frac{\partial}{\partial t'}\rho = -i[H_D, \rho] - \Gamma\rho. \quad (29)$$

Here we have not explicitly written the dependence of the operators on the nuclear coordinate θ. Note that all operators are also operators in the four-dimensional electronic Hilbert space. In the basis of electronic eigenstates of the dimer Hamiltonian, Eq. (29) becomes

$$\dot{\rho}_{kl} = -i(H_k(\theta)\rho_{kl} - \rho_{kl}H_l(\theta)) - \sum_{m,n} \Gamma_{kl,mn}(\theta)\rho_{mn} \quad (30)$$

with $\rho_{kl} = \langle k|\rho|l\rangle$ and $\{k, l\} \in \{\mathbf{g}, \mathbf{b_1}, \mathbf{b_2}, \mathbf{f}\}$. H_k and H_l are given in Eq. (8).

V. MIXED QUANTUM/CLASSICAL DESCRIPTION

To evaluate the response functions, we will use a mixed quantum/classical description where the electronic degrees of freedom evolve quantum mechanically under the influence of nuclear motion, which is treated classically. We describe the dynamics of the nuclear coordinates by classical trajectories with a time evolution governed by an Ehrenfest type of equation.[36] Thereby the nuclear motion takes place on an averaged potential $U(\theta)$. The specific form of this potential depends on whether populations of electronic states or coherences between them are considered and will be given later in Eqs. (39) and (40).

For a given potential $U(\theta)$ the equation of motion for the classical angle $\theta(t)$ reads

$$I\frac{\partial^2}{\partial t'}\theta(t') = -\frac{\partial}{\partial\theta}U(\theta), \tag{31}$$

where I is the moment of inertia, which was introduced in Sec. II B.

The equation of motion in the electronic Hilbert space is

$$\dot{\rho}_{kl}(t') = -i\omega_{kl}(\theta(t'))\rho_{kl}(t') - \sum_{m,n}\Gamma_{kl,mn}(\theta(t'))\rho_{mn}(t'), \tag{32}$$

where

$$\omega_{kl}(\theta(t')) = V_k(\theta(t')) - V_l(\theta(t')) \tag{33}$$

denotes the transition frequency between the adiabatic potentials V_k and V_l at the torsional angle $\theta(t')$.

In the mixed quantum/classical description the operators $\vec{\mu}$ and $\mathcal{G}$ appearing in the response functions (25)–(28) become functions of the time-dependent angle $\theta(t')$. Then, for example, $\vec{\mu}_{nm}(\theta(\tau_3+\tau_2+\tau_1))$ from Eq. (25) is the transition dipole moment between the electronic states m and n, evaluated at the torsional angle which has been reached at time $\tau_3+\tau_2+\tau_1$. Similar, in the tensor elements of the Green-functions, e.g., $\mathcal{G}_{mn,il}(\tau_3)$, the torsional angle $\theta(\tau_3+\tau_2+\tau_1)$ enters parametrically besides the explicit dependence on τ_3.

A. Approximations within the mixed quantum/classical description

In the following, we give further details how the mixed quantum/classical propagation is evaluated. To obtain simple expressions we will introduce some additional approximations.

Within the secular approximation[37] we will assume that the "relaxation operator" Γ does not couple coherences with populations and different coherences. Furthermore relaxation is only taken into account within the one-exciton space. Thus, the only non-vanishing elements in Eq. (30) are

$$\Gamma_{kl,kl}, \quad k \neq l, \tag{34}$$

$$\Gamma_{kk,ll}, \quad k \neq l, k, l \in \{\mathbf{b_1}, \mathbf{b_2}\}, \tag{35}$$

$$\Gamma_{kk,kk}, \quad k \in \{\mathbf{g}, \mathbf{b_1}, \mathbf{b_2}, \mathbf{f}\}. \tag{36}$$

Then the relaxation of populations and the dephasing of coherences can be treated separately according to the formulas

$$\dot{\rho}_{mm}(t') = \sum_k -\Gamma_{mmkk}(\theta(t'))\rho_{kk}(t') \tag{37}$$

and (for $k \neq l$)

$$\dot{\rho}_{kl}(t') = -i\omega_{kl}(\theta(t'))\rho_{kl}(t') - \Gamma_{kl,kl}(\theta(t'))\rho_{kl}(t'). \tag{38}$$

If different eigenstates of the system are populated, we take the potential $U(\theta)$ as the average

$$U(\theta) = \bar{U}(\theta) = \sum_k V_k(\theta)\rho_{kk} \tag{39}$$

of the adiabatic potential surfaces $V_k(\theta)$, weighted with the populations ρ_{kk}.

If the considered Liouville-space pathway contains a coherence $|k\rangle\langle l|$, we propagate with the potential

$$U(\theta) = \frac{1}{2}(V_k(\theta) + V_l(\theta)). \tag{40}$$

A more sophisticated treatment using, e.g., surface hopping methods would allow to consider the combined nuclear-exciton dynamics in more detail. However the simple model introduced above allows already to identify many general features.

In the following we will discuss how we treat the dynamics during the three time periods τ, T, and t.

1. Evolution during coherence and detection time, τ and t

During the relatively short delay times τ and t (which are on the femtosecond timescale) compared to the time needed for complete relaxation (in the picosecond range), we take the nuclear position as fixed at $\theta(0)$ and $\theta(\tau+T)$, respectively. This assumption leads to the Green-functions

$$\mathcal{G}(\tau) = \Theta(\tau)\exp(-i\mathcal{L}(\theta(0))\tau) \tag{41}$$

during the time interval τ and

$$\mathcal{G}(t) = \Theta(t)\exp(-i\mathcal{L}(\theta(\tau+T))t) \tag{42}$$

during the time interval t. Note that these are operators only with respect to electronic degrees of freedom, since we fixed the nuclear coordinate.

2. Evolution during the population time T

For the propagation during the population time, the Green-function is obtained from

$$\mathcal{G}(T) = \Theta(T)\exp\left(-i\int_\tau^{T+\tau}\mathcal{L}(\theta(t'))dt'\right). \tag{43}$$

As mentioned above, within the secular approximation relaxation of populations and dephasing of coherences can be treated separately.

a. Dephasing. In this case we consider $\mathcal{G}_{abcd}$ with $a=c$, $b=d$ and $a \neq b$. Then the Liouville-von-Neumann equation (Eq. (29)) takes the form given in Eq. (38). A simple solution is possible due to the special form of the potential for the

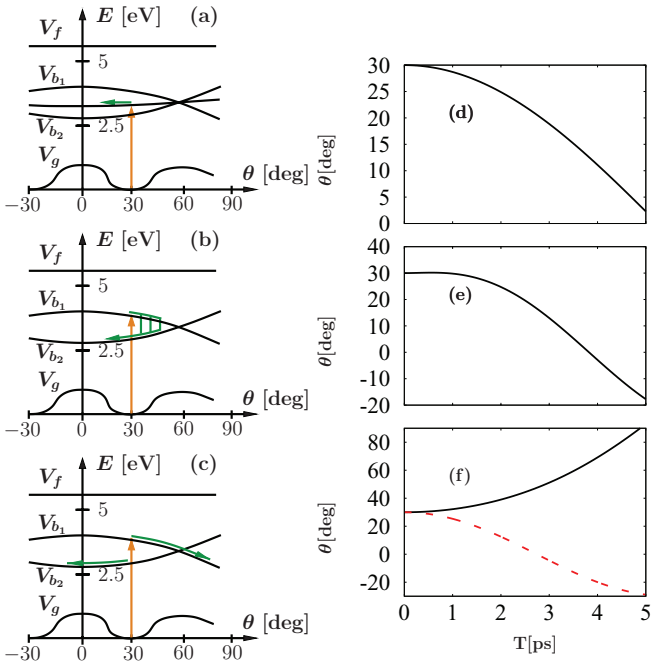

FIG. 4. Sketch of the potential surfaces with illustration of the torsional dynamics during the population time and the corresponding time-dependence of θ for different cases. (a) and (d) Torsional motion on the averaged potential while the system resides in a coherence between the singly excited states $\mathbf{b_1}$ and $\mathbf{b_2}$. (b) and (e) Relaxation of the $\mathbf{b_1}$ population takes place due to system-bath interaction. (c) and (f) Torsional motion takes place through the curve crossing. The solid (black) curves are for initial population in $V_{\mathbf{b_1}}$, the dashed (red) curve is for initial population in $V_{\mathbf{b_2}}$.

classical motion $U_{kl}(\theta) = \frac{1}{2}(V_k(\theta) + V_l(\theta))$, which does not depend on the density matrix ρ. The classical motion is performed independent of the electronic propagation. The trajectory $\theta(t')$ obtained in this way can then be inserted into the response functions (see Eqs. (63)–(66)).

The matrix elements (for $k \neq l$) of the Green-operator are then given by

$$\mathcal{G}_{klkl}(T) = \Theta(T)\exp\{-i\varphi(T)\} \tag{44}$$

with $\varphi(T) = \int_{\tau}^{T+\tau}(\omega_{kl}(\theta(t')) - i\Gamma_{kl,kl}(\theta(t')))dt'$.

For an illustration of the torsional motion during the population time if a coherence between the singly excited states appears in the respective Liouville-space pathway, see left hand side of Fig. 4.

b. Relaxation. Now we are interested in $\mathcal{G}_{aabb}$. As said before we assume that the populations do not couple to coherences. Thus, the Liouville-von-Neumann equation (Eq. (29)) takes the form given in Eq. (37). Since we assume that relaxation only takes place in the one-exciton space, i.e., between the states $|\mathbf{b_1}\rangle$ and $|\mathbf{b_2}\rangle$, we define the transition rates $k_{\mathbf{b_1}} = -\Gamma_{\mathbf{b_2b_2b_1b_1}} = +\Gamma_{\mathbf{b_1b_1b_1b_1}}$, $k_{\mathbf{b_2}} = -\Gamma_{\mathbf{b_1b_1b_2b_2}} = +\Gamma_{\mathbf{b_2b_2b_2b_2}}$, and $\Gamma_{mmkk} = 0$ for other values of m and k. Then

$$\begin{aligned}\frac{\partial}{\partial t'}\rho_{\mathbf{b_1b_1}}(t') &= -k_{\mathbf{b_1}}\rho_{\mathbf{b_1b_1}}(t') + k_{\mathbf{b_2}}\rho_{\mathbf{b_2b_2}}(t'),\\ \frac{\partial}{\partial t'}\rho_{\mathbf{b_2b_2}}(t') &= k_{\mathbf{b_1}}\rho_{\mathbf{b_1b_1}}(t') - k_{\mathbf{b_2}}\rho_{\mathbf{b_2b_2}}(t').\end{aligned} \tag{45}$$

In the more general case we consider first, relaxation takes place due to interactions with the surrounding bath and is not restricted to certain positions of the torsional angle. Here, from detailed balance, we take

$$\frac{k_{\mathbf{b_2}}(\theta)}{k_{\mathbf{b_1}}(\theta)} = \exp[-\hbar\omega_{\mathbf{b_1b_2}}(\theta)/k_BT], \tag{46}$$

where T is the temperature and k_B the Boltzmann constant. For simplicity, we assume zero temperature, so that $k_{\mathbf{b_2}} = 0$. Furthermore we take $k_{\mathbf{b_1}}$ as constant. If $k_{\mathbf{b_1}}$ and $k_{\mathbf{b_2}}$ are independent of θ, a simple analytic solution is possible and one obtains

$$\mathcal{G}_{jjnn}(T) = \left[\begin{pmatrix} 1 & 0 & 0 & 0\\ 0 & \frac{k_{\mathbf{b_1}}f(T)+k_{\mathbf{b_2}}}{k_{\mathbf{b_1}}+k_{\mathbf{b_2}}} & -\frac{k_{\mathbf{b_2}}(f(T)-1)}{k_{\mathbf{b_1}}+k_{\mathbf{b_2}}} & 0\\ 0 & -\frac{k_{\mathbf{b_1}}(f(T)-1)}{k_{\mathbf{b_1}}+k_{\mathbf{b_2}}} & \frac{k_{\mathbf{b_2}}f(T)+k_{\mathbf{b_1}}}{k_{\mathbf{b_1}}+k_{\mathbf{b_2}}} & 0\\ 0 & 0 & 0 & 1 \end{pmatrix}\right]_{jn} \tag{47}$$

with $f(T) = \exp(-(k_{\mathbf{b_1}} + k_{\mathbf{b_2}})T)$.

In contrast to the case of Eq. (40), now the electronic evolution is coupled to the nuclear motion via the potential $\bar{U} = V_{\mathbf{b_1}}\rho_{\mathbf{b_1b_1}} + V_{\mathbf{b_2}}\rho_{\mathbf{b_2b_2}}$, which leads to the classical equation of motion

$$I\ddot{\theta}(t') = -\big(\partial_\theta V_{\mathbf{b_1}}(\theta(t'))\rho_{\mathbf{b_1b_1}}(t') + \partial_\theta V_{\mathbf{b_2}}(\theta(t'))\rho_{\mathbf{b_2b_2}}(t')\big). \tag{48}$$

A sketch of torsional motion when the dimer is in a coherence between the one-exciton states is given in the middle panel of Fig. 4. Note that this figure is just aimed to illustrate schematically that during torsional motion population transfer takes place. A more precise illustration of the population evolution combined with torsional motion is given in Fig. 7.

c. Torsional motion through the curve crossing. We will treat the influence of the CC in such a way, that torsional motion completely passes through the intersection. To see the dynamics associated with torsional motion more clearly, we ignore relaxation processes upon system-bath interactions.

Then, if $\mathbf{b_1}$ is populated initially, the equation of motion reads

$$I\ddot{\theta}(t') = -\frac{\partial}{\partial\theta}V_{\mathbf{b_1}}(\theta(t')). \tag{49}$$

and $\mathcal{G}_{jj\mathbf{b_1b_1}}(T) = \delta_{j\mathbf{b_1}}$ with $j = \mathbf{b_1}, \mathbf{b_2}$.

In the case of an initial population of $\mathbf{b_2}$, the propagation is performed solely on the lower surface according to

$$I\ddot{\theta}(t') = -\partial_\theta V_{\mathbf{b_2}}(\theta(t')) \tag{50}$$

and $\mathcal{G}_{jj\mathbf{b_2b_2}}(T) = \delta_{j\mathbf{b_2}}$ for $j = \mathbf{b_1}, \mathbf{b_2}$.

B. The final response functions

In the following, we use the rotating wave approximation to reduce the number of summations in the response functions (Eqs. (25)–(28)) by keeping only transitions with energies resonant with the laser frequency. Thereby we make use

of the fact that the central frequency of the pulses is that of the monomeric electronic transition energy, which is much larger than the splitting between the singly excited dimer states. Furthermore, the energetic pulse width is assumed to cover both singly excited state potentials in the whole range of θ, while it is much smaller than the other energy differences between electronic states. The response functions after RWA are given in Appendix A together with an assignment to a temporal sequence of the three pulses (which are assumed to be non-overlapping). According to Eq. (18) the final 2D-spectrum is obtained from a two-dimensional Fourier-transformation with respect to τ and t.

For convenience we define the "line-shape" function

$$\mathcal{G}^{(\pm)}_{ij,ij}(\omega;t') = i[\pm\omega - \omega_{ij}(\theta(t')) + i\Gamma_{ij}]^{-1}, \tag{51}$$

where the second argument t' denotes the time at which the angle θ is evaluated.

In the following, we will not be interested in double coherence contributions, which are located at energies corresponding to the sum of the eigenenergies of the one-exciton states at the position of the ground-state minimum. Therefore, in this section we will concentrate on the response functions R_1, R_2, R_1^*, R_2^*, R_3, and R_4. For completeness formulas for R_3^* and R_4^* can be found in Appendix B.

We start with the response functions R_3 and R_4. In these response functions the system evolves in the ground state $\mathbf{g}$ during the population time T. After orientational averaging, one has

$$\begin{aligned} R_3(\omega_\tau, T, \omega_t) = & \sum_{\substack{\{i,j\}\\ \in\{\mathbf{b_2},\mathbf{b_1}\}}} \mathcal{O}_{ij}\ \mu_{\mathbf{g}j}\mathcal{G}^{(+)}_{j\mathbf{g},j\mathbf{g}}(\omega_t;T)\,\mu_{j\mathbf{g}} \\ & \times \mathcal{G}_{\mathbf{gggg}}(T)\,\mu_{\mathbf{g}i} \\ & \times \mathcal{G}^{(-)}_{\mathbf{g}i,\mathbf{g}i}(\omega_\tau;0)\mu_{i\mathbf{g}}, \end{aligned} \tag{52}$$

$$\begin{aligned} R_4(\omega_\tau, T, \omega_t) = & \sum_{\substack{\{i,j\}\\ \in\{\mathbf{b_2},\mathbf{b_1}\}}} \mathcal{O}_{ij}\ \mu_{\mathbf{g}j}\mathcal{G}^{(+)}_{j\mathbf{g},j\mathbf{g}}(\omega_t;T)\,\mu_{j\mathbf{g}} \\ & \times \mathcal{G}_{\mathbf{gggg}}(T)\,\mu_{\mathbf{g}i} \\ & \times \mathcal{G}^{(+)}_{i\mathbf{g},i\mathbf{g}}(\omega_\tau;0)\,\mu_{i\mathbf{g}}. \end{aligned} \tag{53}$$

In the formulas above the bold subscripts $\mathbf{g}$ denote the electronic ground state and

$$\mathcal{O}_{ij} = \frac{1}{5}\delta_{ij} + \frac{1}{15}(1-\delta_{ij}) \tag{54}$$

appears due to the orientational averaging as described in Appendix B. Thus, diagonal peaks ($i = j$) are weighted three times as much as cross-peaks ($i \neq j$).

The response functions R_3 and R_4 from Eqs. (52) and (53) are termed "ground state bleaching" (GSB) contributions; the system resides in a ground state population after the second pulse. This property is a distinguishing feature compared to "excited state emission" (ESE) and "excited state absorption" (ESA) contributions, where the system resides in the singly excited state manifold during the population time. The ESE contribution consists of the response functions R_1 and R_2, the ESA contribution comprises the terms R_1^* and R_2^*. A more detailed discussion of the respective contributions is given, e.g., in Ref. 38. For later use we will divide each of the latter response functions into two parts which we denote by "relaxation part" and "dephasing part" depending on whether the evolution of population or coherence contributions during the time T in terms of the respective Liouville-space pathway is considered:

$$\tilde{R}_1(\omega_\tau, T, \omega_t) = \tilde{R}^{\text{relax}}_{+;\mathbf{g}}(\omega_\tau, T, \omega_t) + \tilde{R}^{\text{deph}}_{+;\mathbf{g}}(\omega_\tau, T, \omega_t), \tag{55}$$

$$\tilde{R}_2(\omega_\tau, T, \omega_t) = \tilde{R}^{\text{relax}}_{-;\mathbf{g}}(\omega_\tau, T, \omega_t) + \tilde{R}^{\text{deph}}_{-;\mathbf{g}}(\omega_\tau, T, \omega_t), \tag{56}$$

$$\tilde{R}_1^*(\omega_\tau, T, \omega_t) = \tilde{R}^{\text{relax}}_{-;\mathbf{f}}(\omega_\tau, T, \omega_t) + \tilde{R}^{\text{deph}}_{-;\mathbf{f}}(\omega_\tau, T, \omega_t), \tag{57}$$

$$\tilde{R}_2^*(\omega_\tau, T, \omega_t) = \tilde{R}^{\text{relax}}_{+;\mathbf{f}}(\omega_\tau, T, \omega_t) + \tilde{R}^{\text{deph}}_{+;\mathbf{f}}(\omega_\tau, T, \omega_t), \tag{58}$$

where

$$\begin{aligned} \tilde{R}^{\text{relax}}_{+;\mathbf{g}}(\omega_\tau, T, \omega_t) = & \sum_{\substack{\{i,j\}\\ \in\{\mathbf{b_2},\mathbf{b_1}\}}} \mathcal{O}_{ij}\ (\vec{\mu}_{\mathbf{g}i})_\alpha \mathcal{G}^{(+)}_{i\mathbf{g},i\mathbf{g}}(\omega_t;T)\,(\vec{\mu}_{\mathbf{g}i})_\beta \\ & \times \mathcal{G}_{ii,jj}(T)\,(\vec{\mu}_{j\mathbf{g}})_\gamma \mathcal{G}^{(+)}_{j\mathbf{g},j\mathbf{g}}(\omega_\tau;0)\,(\vec{\mu}_{j\mathbf{g}})_\delta, \end{aligned} \tag{59}$$

$$\begin{aligned} \tilde{R}^{\text{relax}}_{-;\mathbf{g}}(\omega_\tau, T, \omega_t) = & \sum_{\substack{\{i,j\}\\ \in\{\mathbf{b_2},\mathbf{b_1}\}}} \mathcal{O}_{ij}\ (\vec{\mu}_{\mathbf{g}i})_\alpha \mathcal{G}^{(+)}_{i\mathbf{g},i\mathbf{g}}(\omega_t;T)\,(\vec{\mu}_{\mathbf{g}i})_\beta \\ & \times \mathcal{G}_{ii,jj}(T)\,(\vec{\mu}_{j\mathbf{g}})_\gamma \mathcal{G}^{(-)}_{\mathbf{g}j,\mathbf{g}j}(\omega_\tau;0)\,(\vec{\mu}_{\mathbf{g}j})_\delta, \end{aligned} \tag{60}$$

$$\begin{aligned} \tilde{R}^{\text{relax}}_{+;\mathbf{f}}(\omega_\tau, T, \omega_t) = & \sum_{\substack{\{i,j\}\\ \in\{\mathbf{b_2},\mathbf{b_1}\}}} \mathcal{O}_{ij}\ (\vec{\mu}_{\mathbf{f}i})_\alpha \mathcal{G}^{(+)}_{\mathbf{f}i,\mathbf{f}i}(\omega_t;T)\,(\vec{\mu}_{\mathbf{f}i})_\beta \\ & \times \mathcal{G}_{ii,jj}(T)\,(\vec{\mu}_{j\mathbf{g}})_\gamma \mathcal{G}^{(+)}_{j\mathbf{g},j\mathbf{g}}(\omega_\tau;0)\,(\vec{\mu}_{j\mathbf{g}})_\delta, \end{aligned} \tag{61}$$

$$\begin{aligned} \tilde{R}^{\text{relax}}_{-;\mathbf{f}}(\omega_\tau, T, \omega_t) = & \sum_{\substack{\{i,j\}\\ \in\{\mathbf{b_2},\mathbf{b_1}\}}} \mathcal{O}_{ij}\ (\vec{\mu}_{\mathbf{f}i})_\alpha \mathcal{G}^{(+)}_{\mathbf{f}i,\mathbf{f}i}(\omega_t;T)\,(\vec{\mu}_{\mathbf{f}i})_\beta \\ & \times \mathcal{G}_{ii,jj}(T)\,(\vec{\mu}_{j\mathbf{g}})_\gamma \mathcal{G}^{(-)}_{\mathbf{g}j,\mathbf{g}j}(\omega_\tau;0)\,(\vec{\mu}_{\mathbf{g}j})_\delta, \end{aligned} \tag{62}$$

and

$$\begin{aligned} \tilde{R}^{\text{deph}}_{+;\mathbf{g}}(\omega_\tau, T, \omega_t) = & \sum_{\substack{\{i\neq j\}\\ \in\{\mathbf{b_2},\mathbf{b_1}\}}} (1/15)\ (\vec{\mu}_{\mathbf{g}i})_\alpha \mathcal{G}^{(+)}_{i\mathbf{g},i\mathbf{g}}(\omega_t;T)\,(\vec{\mu}_{\mathbf{g}j})_\beta \\ & \times \mathcal{G}_{ij,ij}(T)\,(\vec{\mu}_{\mathbf{g}j})_\gamma \mathcal{G}^{(+)}_{i\mathbf{g},i\mathbf{g}}(\omega_\tau;0)\,(\vec{\mu}_{i\mathbf{g}})_\delta, \end{aligned} \tag{63}$$

$$\begin{aligned} \tilde{R}^{\text{deph}}_{-;\mathbf{g}}(\omega_\tau, T, \omega_t) = & \sum_{\substack{\{i\neq j\}\\ \in\{\mathbf{b_2},\mathbf{b_1}\}}} (1/15)\ (\vec{\mu}_{\mathbf{g}i})_\alpha \mathcal{G}^{(+)}_{i\mathbf{g},i\mathbf{g}}(\omega_t;T)\,(\vec{\mu}_{\mathbf{g}j})_\beta \\ & \times \mathcal{G}_{ij,ij}(T)\,(\vec{\mu}_{i\mathbf{g}})_\gamma \mathcal{G}^{(-)}_{\mathbf{g}j,\mathbf{g}j}(\omega_\tau;0)\,(\vec{\mu}_{\mathbf{g}j})_\delta, \end{aligned} \tag{64}$$

$$\begin{aligned} \tilde{R}^{\text{deph}}_{+;\mathbf{f}}(\omega_\tau, T, \omega_t) = & \sum_{\substack{\{i\neq j\}\\ \in\{\mathbf{b_2},\mathbf{b_1}\}}} -(1/15)\ (\vec{\mu}_{\mathbf{f}j})_\alpha \mathcal{G}^{(+)}_{\mathbf{f}j,\mathbf{f}j}(\omega_t;T)\,(\vec{\mu}_{\mathbf{f}i})_\beta \\ & \times \mathcal{G}_{ij,ij}(T)\,(\vec{\mu}_{\mathbf{g}j})_\gamma \mathcal{G}^{(+)}_{i\mathbf{g},i\mathbf{g}}(\omega_\tau;0)\,(\vec{\mu}_{i\mathbf{g}})_\delta, \end{aligned} \tag{65}$$

$$\tilde{R}^{\mathrm{deph}}_{-;\mathbf{f}}(\omega_\tau, T, \omega_t) = \sum_{\substack{\{i\neq j\}\\ \in\{\mathbf{b_2},\mathbf{b_1}\}}} -(1/15)\,(\vec{\mu}_{\mathbf{f}j})_\alpha \mathcal{G}^{(+)}_{\mathbf{f}j,\mathbf{f}j}(\omega_t; T)\,(\vec{\mu}_{\mathbf{f}i})_\beta \times \mathcal{G}_{ij,ij}(T)\,(\vec{\mu}_{i\mathbf{g}})_\gamma \mathcal{G}^{(-)}_{\mathbf{g}j,\mathbf{g}j}(\omega_\tau; 0)\,(\vec{\mu}_{\mathbf{g}j})_\delta. \tag{66}$$

In the latter equations, the factors $\mathcal{O}_{ij}$ (defined in Eq. (54)) and $\pm\frac{1}{15}$ stem from orientational averaging. Each Green operator and each transition dipole is evaluated at a certain angle. The rightmost transition dipole operators and the Green operator between them are evaluated at the angle $\theta(0) = \theta_0$. All other terms are evaluated at $\theta(T)$. Note that the value $\theta(T)$ depends on the specific path. We have divided the latter response function in relaxation and dephasing terms to facilitate the interpretation of the 2D spectra presented in Sec. VI.

The relaxation parts of the response functions are characterized by the indices *iijj* of the Green-propagator related to the population time interval. Thus, the first and the last pair of interactions includes the same transition dipole moments (pattern *mmnn* with $\{m, n\} \in \{\vec{\mu}_I, \vec{\mu}_{II}\}$ according to the definitions from Eqs. (11) and (12), where *m* and *n* can either be equal or not). On the other hand, the dephasing parts characterized by the indices *ijij* of the Green-tensor during *T* allows either the interaction pattern *mnnm* ($\tilde{R}^{\mathrm{deph}}_{+;\mathbf{g}}$ and $\tilde{R}^{\mathrm{deph}}_{-;\mathbf{f}}$) or *mnmn* ($\tilde{R}^{\mathrm{deph}}_{-;\mathbf{g}}$ and $\tilde{R}^{\mathrm{deph}}_{+;\mathbf{f}}$) with $m \neq n$. Note that in the final 2D spectrum, peak positions are determined by the poles of $\mathcal{G}(\omega_\tau; T)$ and $\mathcal{G}(\omega_t; 0)$, which are located at the energy differences of the first and the final transition.

VI. MODEL CALCULATIONS

A. Used parameter values

We present the results of our model calculation with specific attention to the question how underlying dissipative processes can be identified on the basis of features in the 2D-spectra. For this aim we study the evolution of 2D-spectra as a function of the population time *T*. To identify clear signatures of relaxation and torsional motion we focus on two limiting cases:

(1) Relaxation between the two singly excited states is much faster than the time needed to reach the CC.
(2) Relaxation between the two singly excited states is much slower than the time needed to reach the CC. Direct relaxation due to interactions with the bath is neglected in this case. We assume torsional motion to completely pass through the CC.

For our chosen potential surfaces the time T^* to reach the crossing at $\theta = 30^\circ$ is roughly 3.5 ps.

For the calculations presented below the dephasing constants and the relaxation rates have been chosen as follows: For dephasing between singly excited states (see Eq. (38)) we take $\Gamma \equiv \Gamma_{kl,\,kl} = 1\,\mathrm{ps}^{-1} = 3.534/T^*$. The other dephasing constants are set to $\Gamma \equiv \Gamma_{kl,\,kl} = 40\,\mathrm{ps}^{-1} = 141.36/T^*$.

For direct relaxation (see Eq. (45)) we take $k_{\mathbf{b_2}} = 0\,\mathrm{ps}^{-1}$. The rate $k_{\mathbf{b_1}} = 1\,\mathrm{ps}^{-1} = 3.534/T^*$ corresponds to the dephasing rate between the singly excited states $\mathbf{b_1}$ and $\mathbf{b_2}$ in agreement with Ref. 30.

For both situation (1) and (2) we use the same dephasing rates. In case (1) we take nuclear motion into account, but the relaxation is so fast that this effect can hardly be seen.

B. Time-dependence of torsional motion

Before considering the 2D spectra, we first take a look at the time-dependence of torsional motion during the population time *T*. Again, we consider the cases from Sec. V A 2 separately. Based on these dynamics, features in the 2D-spectra can be understood.

a. Coherence between singly excited states: Solving Eq. (38) with the averaged potential Eq. (40) for the parameters specified in Sec. VI A we find the dynamics displayed in Fig. 4(d). The monomers slowly rotate into a parallel orientation. For the chosen values of the dephasing constants the coherences have decayed completely after 3 ps.

b. Population transfer takes place in form of direct relaxation due to interactions with the bath: The time-dependent torsional angle is given in Fig. 4(e). After 2 ps population transfer has almost completely taken place.

c. Torsional motion through the curve crossing takes place: The torsional dynamics subsequent to absorption from $\mathbf{g}$ to $\mathbf{b_1}$ and $\mathbf{b_2}$ is calculated separately (see Fig. 4(f)).

It is worth mentioning once again that we only employ a simplified phenomenological description of the processes at the crossing. In particular, we do not take such trajectories into account, which arise from a change of the potential surface near the crossing point. A detailed discussion of the complex interplay between relaxation and dephasing processes at a curve crossing is given, e.g., in Ref. 39.

C. 2D spectra

In the following we show only the imaginary part of the 2D-spectra (Eq. (18)), as it provides sufficient information about the underlying dissipative processes and torsional motion. 2D spectra related to our model system are presented in Figs. 5 and 6 for different population times *T*.[50] Besides the full spectra (last row) we also show the individual contributions of GSB, ESE, and ESA, since these individual contributions allow a simple understanding of the full spectrum. The DC contributions will be discussed in Appendix C.

The GSB, ESE, and ESA contributions, which add up to the full 2D-spectrum, are assigned to the response functions in terms of

$$S_{\mathrm{GSB}} = R_3 + R_4, \tag{67}$$

$$S_{\mathrm{ESE}} = R_1 + R_2, \tag{68}$$

$$S_{\mathrm{ESA}} = -R_1^* - R_2^*, \tag{69}$$

i.e., each contribution contains a rephasing and a non-rephasing response function.

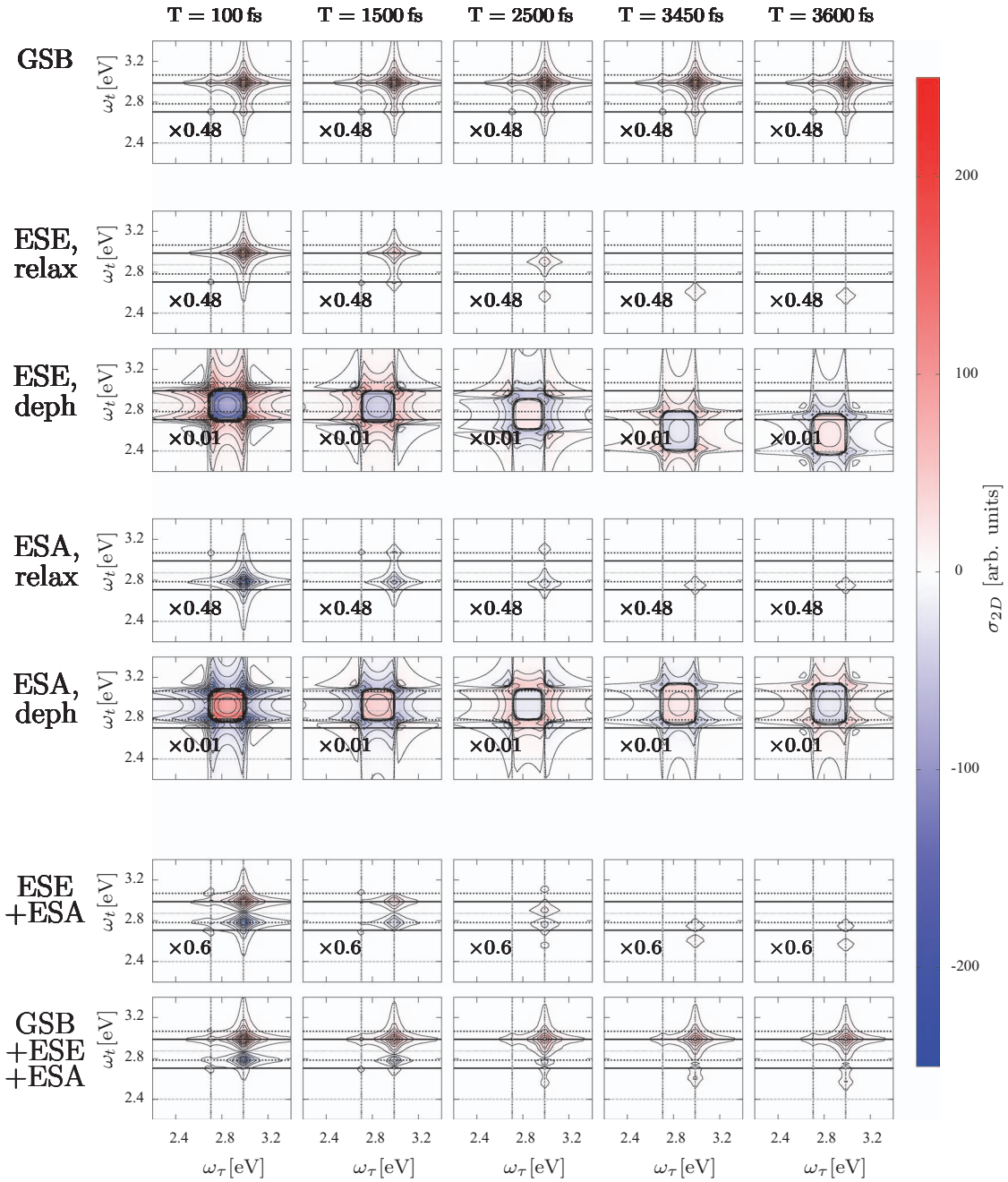

FIG. 5. Contributions to the 2D-spectrum in the case of direct relaxation: GSB (first row), relaxation part of ESE (second row), dephasing part of ESE (second row), relaxation part of ESA (fourth row), dephasing part of ESA (fifth row), complete 2D-spectrum without GSB (sixth row), and complete 2D-spectrum (seventh row). The contour lines indicate peak intensity levels within the interval between $-I_{max}$ and I_{max} with an incremental step size of $0.1I_{max}$ and additional levels at $-0.05I_{max}$, $-0.01I_{max}$, $0.01I_{max}$, and $0.05I_{max}$, where I_{max} denotes the maximal absolute value of the 2D-spectra in the respective row of the figure.

The double coherence contribution is given by

$$S_{\mathrm{DC}} = -R_3^* - R_4^*. \tag{70}$$

In order to make also low-intensity structures visible, we apply a scaling of the data points of the 2D-spectrum $\sigma_{2D}(\omega_\tau, \omega_t)$ by the function $arcsinh(f \cdot \sigma_{2D}(\omega_\tau, \omega_t))$ with $f = 10$.

In each plot the horizontal and vertical lines indicate the relevant energy differences of the problem considered. As ω_τ corresponds to the absorption frequency related to the first transition, vertical lines at the energy difference between the ground state and the states $\mathbf{b_1}$ and $\mathbf{b_2}$ at the initial angle 30° are shown. The same holds for the ω_t-coordinate, where the respective energy values are indicated by solid black lines. In Sec. V B it was mentioned that the ω_t-position of spectral features corresponds to the energy difference related to the final transition. Because of possible position change of the torsional angle during the population time, this energy difference can be modified compared to the initial position. Furthermore, the doubly excited state is involved in ESA processes, so that additional transition energies appear due to the different slopes of ground-state and doubly excited state potential. The horizontal gray dashed line at ∼2.4 eV indicates the energy difference between the ground-state potential and the CC (at 60°). Furthermore, the two horizontal dotted black lines

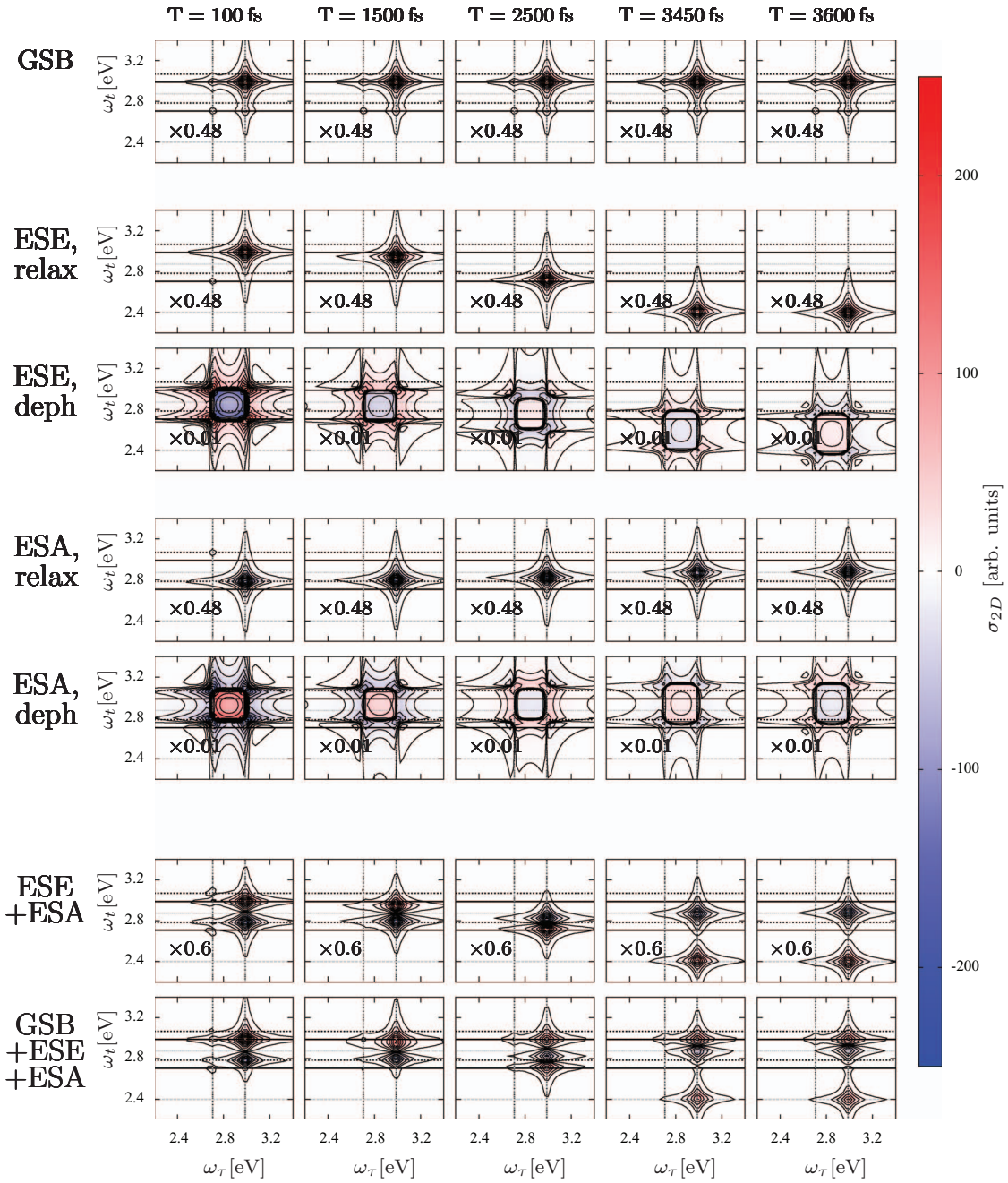

FIG. 6. Same as Fig. 5 but now for the case of torsional motion through the curve crossing.

indicate the transition energies of the states $\mathbf{b_1}$ and $\mathbf{b_2}$ at the initial angle 30° to the doubly excited state. By the gray short-dashed line between 2.8 eV and 3.0 eV the energy difference between the CC and the doubly excited state is marked.

Before discussing the full 2D spectrum we first consider the components separately.

1. Ground state bleaching

The first line of both figures shows the GSB contribution. The first thing to note is that for both situations (1) and (2) the GSB spectra are identical and independent of the population time T. This can be easily understood from Eqs. (52) and (53): Since we have assumed that the torsional motion can be neglected during coherence time τ and during detection time t, the system will stay during the population time T at the initial angle, and no torsional dynamic takes place. Then in both cases the Green function $\mathcal{G}_{\mathbf{gggg}} = 1$ appears (since we have taken the corresponding energy as the zero of energy). Thus, the GSB signal exhibits peaks located at the four positions $(\omega_{\mathrm{b}_{1/2}\mathbf{g}}, \omega_{\mathrm{b}_{1/2}\mathbf{g}})$, which are just the crossing points of the solid black lines. The different peaks have a large intensity difference, because the relative intensities are determined by the ratio of the absolute values of the involved transition dipole moments $\vec{\mu}_{\mathbf{gb_1}}$ and $\vec{\mu}_{\mathbf{gb_2}}$, which at the initial angle have a ratio of roughly 3.7. Therefore only a remanescence of the lower diagonal peak is visible.

While the GSB contribution yields no information about the dynamics in the singly excited state manifold, ESE and ESA reflect the relaxation and dephasing processes in the 1-exciton basis and the related torsional motion during the population time.

2. ESE and ESA

For the purpose of easier interpretation, ESE (second and third row) and ESA (fourth and fifth row) contributions to the 2D-spectrum are further separated with respect to coherences and populations evolving during T. For a better assessment, we also provide the time in units of T^*, the time needed to reach the CC.

a. Excited state emission. We first consider ESE. For both direct relaxation and torsional motion through the crossing, the signal associated with being in a coherence during the population time T is identical (see third line of Figs. 5 and 6). However, for the relaxation part (second line) there are clear differences visible between the direct relaxation and the torsional motion through the curve-crossing. For small times $T \approx 100\,\text{fs} = 0.028\,T^*$ both signals are still more or less identical, since neither direct relaxation nor torsional motion have taken place to an appreciable extent. The spectra consist of two peaks on the diagonal (at the energies of the $\mathbf{b_1}$ and $\mathbf{b_2}$ states for the initial angle $\theta = 30^\circ$), see also Figs. 4(b) and 4(c).

For population times $T \geq 1500\,\text{fs}$ the situation is quite different: For $T = 1500\,\text{fs} = 0.424\,T^*$ (third column) torsional motion is still negligible ($\theta \approx 30^\circ$) and direct relaxation has nearly completely taken place, resulting in a strong reduction of the peak at $(\omega_\tau, \omega_t) \approx (E_{\mathbf{b_1}}(30^\circ), E_{\mathbf{b_1}}(30^\circ))$ and the appearance of a cross-peak at $(\omega_\tau, \omega_t) \approx (E_{\mathbf{b_1}}(30^\circ), E_{\mathbf{b_2}}(30^\circ))$ in Fig. 5. The amplitude of this cross-peak is also quite low, since in the respective pathway the product $(\mu_{\mathbf{gb_1}})^2(\mu_{\mathbf{gb_2}})^2$ appears, which is small because at $\theta \approx 30^\circ$ the transition dipole moment $\mu_{\mathbf{gb_2}}$ has a small absolute value. Furthermore the weighting factor from the orientational average is for this pathway only 1/15. At even larger population times T, the magnitude of the signal is further decreased (see fourth and fifth column of Fig. 5).

For the corresponding ESE signal in the case that direct relaxation is negligible (Fig. 6), a totally different behavior for times $T \geq 1500\,\text{fs}$ is found. In the following we will focus on the situation where after the second pulse the exciton state $\mathbf{b_1}$ is populated, since this gives the main contribution. The reason for the dominance of the related peak structure is that the ratio of the absolute values of the involved transition dipole moments $\vec{\mu}_{\mathbf{gb_1}}$ and $\vec{\mu}_{\mathbf{gb_2}}$ is significantly larger than 1 and enters with the power of four in the weighting of the $\mathbf{b_1}$- and $\mathbf{b_2}$-population parts of the ESE contribution. At $T = 1500\,\text{fs} = 0.424\,T^*$ we find only small changes compared to $T = 100\,\text{fs} = 0.028\,T^*$. Now the angle has increased to a value of $\theta \approx 35^\circ$ leading to a slight decrease of the energy of the $\mathbf{b_2}$ state and an increase of the ground potential, which is recognizable in the 2D-spectrum in form of a lowering of the peak position in the ω_t direction. At $T = 2500\,\text{fs} = 0.707\,T^*$, this effect is more pronounced, as an increase up to $\theta \approx 45^\circ$ has taken place. For $T = 3450\,\text{fs} = 0.976\,T^*$ the crossing point is nearly reached. The shift to energies below the energetic level of the crossing (at $\omega_t = 2.4\,\text{eV}$, marked by a gray long-dashed line) stems from increased potential energy of the electronic ground state at the position of the crossing (see second row of Figs. 6 and 7, either rightmost position). For $T = 3600\,\text{fs} = 1.019\,T^*$ the crossing point has been passed. For the trajectories without change of the electronic state in the crossing region, which we exclusively take into account, the peak intensities remain unchanged during torsional motion. On the other hand, in the less important case that population transfer occurs near the crossing point, an immediate decrease of the intensity of the eminent peak appears. This effect is due to the different absolute values of the transition dipole moments between the ground state and the excitonic eigenstates in the crossing region and the modified orientational average of the related transition pathways.

Let us briefly come back to the "coherence" contribution. For constant $\theta_0 = 30^\circ$ one finds a symmetric structure of two diagonal- and cross peaks, respectively. All peaks have the same intensity, as they stem from excitation processes based on the same set of transition dipole moments (only the temporal order is different). The diagonal peaks are related to the response function R_1 and are characterized by an excitation sequence of $\vec{\mu}_{i\mathbf{g}}(0)\vec{\mu}_{j\mathbf{g}}(\tau)\vec{\mu}_{j\mathbf{g}}(\tau+T)\vec{\mu}_{i\mathbf{g}}(\tau+T+t)$ with $i, j \in \mathbf{b_1}, \mathbf{b_2}$ and $i \neq j$. The cross peaks are associated with an

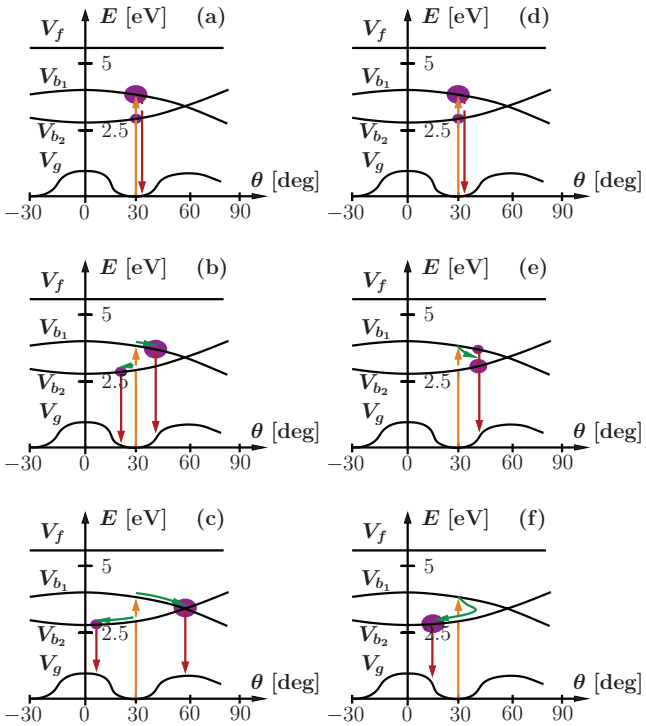

FIG. 7. Excitation schemes at $T = 0\,\text{fs}$ (a, d), $T = 1500\,\text{fs}$ (b, e), and $T = 3600\,\text{fs}$ (c, f) (from left to right) in the cases of torsional motion through the crossing (left column) and direct relaxation (right column). The sizes of the violet discs indicate the relative populations in the respective electronic states. The green arrows can be perceived as the dependence of the potential energy on the torsional angle, which evolves in time.

excitation pattern $\vec{\mu}_{i\mathbf{g}}(0)\vec{\mu}_{j\mathbf{g}}(\tau)\vec{\mu}_{i\mathbf{g}}(\tau+T)\vec{\mu}_{j\mathbf{g}}(\tau+T+t)$, $i, j \in \mathbf{b_1}, \mathbf{b_2}$, $i \neq j$ from R_2 (the dephasing parts of R_1 and R_2 are given in Eqs. (63) and (64)). Note that in the related equations τ and t are set to zero in the arguments of the transition dipole moments because of the frozen torsional motion during those intervals, while both variables are introduced in the previous expressions again in order to allow an assignment of the interactions to the times at which they appear. All four peaks undergo an inversion of phase after 7.275 fs from modulation by a frequency corresponding to potential difference at the initial torsional angle. The signal as a whole decreases with increasing population time due to the influence of the dephasing constant, which leads to a loss of coherence. Furthermore, the position of the four-peak structure as a whole is shifted as a result of motion on the averaged singly excited state potential. Thereby the relative distances between the peaks are modified because of the θ-dependent splitting between the singly excited eigenstates.

b. Excited state absorption. The ESA contribution (row four and five) yields similar information as the ESE contribution. Now, however, the energy differences between the singly excited states and the doubly excited state enter. The relaxation parts of the spectra have opposite (negative) sign compared to the analog ESE contributions because of the negative sign of the complex conjugate counterparts to the individual response function in the expression for the third-order response (Eq. (24)). For the dephasing part of the ESA contribution, the situation is more complicated. There the negative sign of the respective response functions is compensated by the negative sign of the involved transition dipole moment $\vec{\mu}_{\mathbf{fb_2}}$, which only appears once and does therefore not cancel by interacting twice, as in the case of relaxation. Though, due to the negative sign of the orientational averaging factor for ESA contribution, the ESA dephasing parts are nevertheless negative. In the case of ESA, the diagonal peaks and the cross peaks of the dephasing parts stem from the R_2^*- and R_1^*-contribution, respectively (see Eqs. (65) and (66)).

c. The total spectrum. Since experimentally it is difficult to obtain the individual contributions, in the last row the total spectrum, i.e., the sum of all individual contributions, is plotted. Although now the GSB contribution dominates the signal for large population times T, there is still a clear distinction between the two relaxation processes possible. While for direct relaxation quite early ($T < 1500$ fs) no negative contribution is present anymore, in the case where direct relaxation is negligible a negative contribution can be seen. The most striking difference and a clear signature of torsional motion is the continuous movement of the ESE and ESA peaks along the ω_t direction, while in the case of direct relaxation a splitting into two separate peaks appears. To see this effect more clearly it is advantageous to subtract the constant background from the GSB signal. The difference between the complete spectrum and the GSB contribution is shown in the second row from the bottom in Figs. 5 and 6.

VII. SUMMARY AND CONCLUSIONS

We have presented a simple model to investigate different relaxation pathways of a π-aggregated dimer, with particular emphasis on torsional motion. It has been shown that 2D spectroscopy can give insights about the relaxation dynamics. In the following we summarize our findings:

a. Distinction between different ways of relaxation: Concerning the relaxation process, we considered two different cases: On the one hand, in the case of strong interaction of the system with the environment, relaxation from the upper potential occurs before appreciable torsional motion takes place. On the other hand, in the case of weak interaction with the environment, the system can pass the curve crossing due to torsional motion. In the ESE and ESA contributions the two different situations can be clearly distinguished. While the first kind of process leads to a continuous exchange of intensity between the initial diagonal peak at $(\omega_\tau, \omega_t) \approx (E_{\mathbf{b_1}}(\theta(T=0)), E_{\mathbf{b_1}}(\theta(T=0)))$ and a cross peak at $(\omega_\tau, \omega_t) \approx (E_{\mathbf{b_1}}(\theta(T=0)), E_{\mathbf{b_2}}(\theta(T=0)))$ indicating population transfer, the second process merely results in an energetic shift of the initial diagonal peak along the ω_t-axis without involvement of a cross peak. In both cases also a lower diagonal peak appears at $(\omega_\tau, \omega_t) = (E_{\mathbf{b_2}}(\theta(T)), E_{\mathbf{b_2}}(\theta(T)))$, which is low in intensity and unaffected by the relaxation dynamics under the assumption of zero temperature. If the energetically higher 1-exciton potential was steeper, torsional motion would be favored compared to direct relaxation, and the inverse effect is obtained for more flat potentials. On the basis of the characteristic signatures in the 2D-spectra, one can distinguish both relaxation processes, in principle. Note, however, that at the curve crossing one expects strong non-adiabatic couplings, which could lead to direct relaxation just before the curve crossing is reached.

b. Conditions for the appearance of the respective cases: In solution, where strong coupling of the singly excited states to the environment leads to fast relaxation on a timescale much shorter than the time needed to reach the curve crossing in the picosecond range, the first process will appear. The situation with weak coupling to the environment can experimentally be realized in Helium nanodroplets.[10,40] The torsional dynamics could then be studied by spectroscopic techniques as described in Ref. 41, which provide similar 2D signals as the ones considered in the present work. See also the recent discussion in Ref. 34. Our theoretical investigations demonstrate a principle way to draw conclusions about relaxation mechanisms from experimental results.

c. Influence of temperature: We calculated our spectra without regarding static disorder and for zero temperature, where the described effects are clearly visible. At finite temperature, the thermal distribution of the initial angle leads to less distinct peak structures, which makes the evaluation more difficult. Therefore it is advisable to perform the respective measurements at low temperature in order to obtain more pronounced effects.

d. Extraction of relevant components: Although the different contributions to the 2D-spectrum (GSB, ESE, and ESA) on their own allow an uncomplicated interpretation,

it remains challenging to extract them from the sum spectrum. One possible solution is to subtract the GSB contribution, which is independent of the population time, as a constant background. Then the ESE and ESA contributions can be distinguished on the basis of their opposite sign, if the respective peak structures are sufficiently separated from each other. In order to select certain excitation pathways, which are characterized by the pattern of interactions with the transition dipole moments, it is possible to use a combined evaluation of 2D-spectra resulting from differently chosen pulse polarizations. In this way the contributions of populations and coherences can be separated, which allows to investigate dephasing and relaxation effects independent of each other. This approach has been employed, e.g., in Refs. 42–45. Furthermore, it has been suggested that some Liouville pathways can be extracted, using entangled pairs of photons.[46]

Even if the decomposition of measured 2D-spectra into immediately analyzable contributions remains a challenging task, we have shown that, in principle, 2D-spectroscopy is appropriate as a tool to gain insight into the excited state dynamics and the related dissipative phenomena.

ACKNOWLEDGMENTS

Thanks are due to R. Fink for providing results of quantum chemical calculations. Furthermore, we thank S. Wüster, U. Selig, V. Engel, T. Mančal, W. Domcke, and J. Yuen for stimulating discussions. A.E. thanks A. Aspuru-Guzik for the great time. Financial support from the DFG under Contract No. Ei 872/1-1 is acknowledged.

APPENDIX A: THE RESPONSE FUNCTION IN RWA

After the RWA the response functions take the form

$$(\tilde{R}_1)_{\alpha\beta\gamma\delta}(\tau_1,\tau_2,\tau_3) = \sum_{\substack{\{c,h,i,j\}\\ \in\{\mathbf{b_2},\mathbf{b_1}\}}} (\vec{\mu}_{\mathbf{g}i})_\alpha \mathcal{G}_{i\mathbf{g}}(\tau_3)(\vec{\mu}_{\mathbf{g}j})_\beta \mathcal{G}_{ij,ch}(\tau_2) \times (\vec{\mu}_{h\mathbf{g}})_\gamma \mathcal{G}_{c\mathbf{g}}(\tau_1)(\vec{\mu}_{c\mathbf{g}})_\delta, \quad \text{(A1)}$$

$$(\tilde{R}_2)_{\alpha\beta\gamma\delta}(\tau_1,\tau_2,\tau_3) = \sum_{\substack{\{d,g,i,j\}\\ \in\{\mathbf{b_2},\mathbf{b_1}\}}} (\vec{\mu}_{\mathbf{g}i})_\alpha \mathcal{G}_{i\mathbf{g}}(\tau_3)(\vec{\mu}_{\mathbf{g}j})_\beta \mathcal{G}_{ij,gd}(\tau_2) \times (\vec{\mu}_{g\mathbf{g}})_\gamma \mathcal{G}_{\mathbf{g}d}(\tau_1)(\vec{\mu}_{d\mathbf{g}})_\delta, \quad \text{(A2)}$$

$$(\tilde{R}_3)_{\alpha\beta\gamma\delta}(\tau_1,\tau_2,\tau_3) = \sum_{\substack{\{d,k\}\\ \in\{\mathbf{b_2},\mathbf{b_1}\}}} (\vec{\mu}_{\mathbf{g}k})_\alpha \mathcal{G}_{k\mathbf{g}}(\tau_3)(\vec{\mu}_{k\mathbf{g}})_\beta \mathcal{G}_{\mathbf{gg}}(\tau_2) \times (\vec{\mu}_{\mathbf{g}d})_\gamma \mathcal{G}_{\mathbf{g}d}(\tau_1)(\vec{\mu}_{d\mathbf{g}})_\delta, \quad \text{(A3)}$$

$$(\tilde{R}_4)_{\alpha\beta\gamma\delta}(\tau_1,\tau_2,\tau_3) = \sum_{\substack{\{c,k\}\\ \in\{\mathbf{b_2},\mathbf{b_1}\}}} (\vec{\mu}_{\mathbf{g}k})_\alpha \mathcal{G}_{k\mathbf{g}}(\tau_3)(\vec{\mu}_{k\mathbf{g}})_\beta \mathcal{G}_{\mathbf{gg}}(\tau_2) \times (\vec{\mu}_{\mathbf{g}c})_\gamma \mathcal{G}_{c\mathbf{g}}(\tau_1)(\vec{\mu}_{c\mathbf{g}})_\delta, \quad \text{(A4)}$$

$$(\tilde{R}_1^*)_{\alpha\beta\gamma\delta}(\tau_1,\tau_2,\tau_3) = \sum_{\substack{\{d,g,i,j\}\\ \in\{\mathbf{b_2},\mathbf{b_1}\}}} (\vec{\mu}_{j\mathbf{f}})_\alpha \mathcal{G}_{\mathbf{f}j}(\tau_3)(\vec{\mu}_{\mathbf{f}i})_\beta \mathcal{G}_{ij,gd}(\tau_2) \times (\vec{\mu}_{g\mathbf{g}})_\gamma \mathcal{G}_{\mathbf{g}d}(\tau_1)(\vec{\mu}_{d\mathbf{g}})_\delta, \quad \text{(A5)}$$

$$(\tilde{R}_2^*)_{\alpha\beta\gamma\delta}(\tau_1,\tau_2,\tau_3) = \sum_{\substack{\{c,h,i,j\}\\ \in\{\mathbf{b_2},\mathbf{b_1}\}}} (\vec{\mu}_{j\mathbf{f}})_\alpha \mathcal{G}_{\mathbf{f}j}(\tau_3)(\vec{\mu}_{\mathbf{f}i})_\beta \mathcal{G}_{ij,ch}(\tau_2) \times (\vec{\mu}_{h\mathbf{g}})_\gamma \mathcal{G}_{c\mathbf{g}}(\tau_1)(\vec{\mu}_{c\mathbf{g}})_\delta, \quad \text{(A6)}$$

$$(\tilde{R}_3^*)_{\alpha\beta\gamma\delta}(\tau_1,\tau_2,\tau_3) = \sum_{\substack{\{c,l\}\\ \in\{\mathbf{b_2},\mathbf{b_1}\}}} (\vec{\mu}_{l\mathbf{f}})_\alpha \mathcal{G}_{\mathbf{f}l}(\tau_3)(\vec{\mu}_{l\mathbf{g}})_\beta \mathcal{G}_{\mathbf{fg}}(\tau_2) \times (\vec{\mu}_{\mathbf{f}c})_\gamma \mathcal{G}_{c\mathbf{g}}(\tau_1)(\vec{\mu}_{c\mathbf{g}})_\delta, \quad \text{(A7)}$$

$$(\tilde{R}_4^*)_{\alpha\beta\gamma\delta}(\tau_1,\tau_2,\tau_3) = \sum_{\substack{\{d,l\}\\ \in\{\mathbf{b_2},\mathbf{b_1}\}}} (\vec{\mu}_{\mathbf{g}l})_\alpha \mathcal{G}_{l\mathbf{g}}(\tau_3)(\vec{\mu}_{l\mathbf{f}})_\beta \mathcal{G}_{\mathbf{fg}}(\tau_2) \times (\vec{\mu}_{\mathbf{f}d})_\gamma \mathcal{G}_{d\mathbf{g}}(\tau_1)(\vec{\mu}_{d\mathbf{g}})_\delta. \quad \text{(A8)}$$

The involved electronic states are written as bold characters in order to allow a distinction from indices of the same letter. The so-called non-rephasing contributions are characterized by a pulse sequence, where pulse 2 is followed by pulse 1 and finally pulse 3 (short notation: $2-1-3$). For the rephasing contributions a sequence of $1-2-3$ is characteristic. Double coherence contributions are related to the sequence $3-2-1$.

An assignment of the response functions to different kinds of Liouville space pathways is possible. Under the chosen detection direction the contributions of excited state emission ($(\tilde{R}_1)_{\alpha\beta\gamma\delta}$ and $(\tilde{R}_2)_{\alpha\beta\gamma\delta}$) and ground state bleaching ($(\tilde{R}_3)_{\alpha\beta\gamma\delta}$ and $(\tilde{R}_4)_{\alpha\beta\gamma\delta}$) only include transitions between the electronic ground state (**g**) and the singly excited state manifold ($\mathbf{b_1}$ and $\mathbf{b_2}$), for excited state absorption ($(\tilde{R}_1^*)_{\alpha\beta\gamma\delta}$ and $(\tilde{R}_2^*)_{\alpha\beta\gamma\delta}$) and double coherence processes ($(\tilde{R}_3^*)_{\alpha\beta\gamma\delta}$ and respective contribution to $(\tilde{R}_4)_{\alpha\beta\gamma\delta}$) also the doubly excited state (**f**) is involved. A notation using additional subscript symbols for the appearance of excitations, where besides the singly excited states exclusively to the ground state or also to the doubly excited state is involved, can be introduced according to Ref. 47. Using this notation, the rephasing and non-rephasing contributions are identified as

$$S^{(3)}_{\mathrm{R,rw}} = (\tilde{R}_{2g}) + (\tilde{R}_{3g}) - (\tilde{R}^*_{1f}), \quad \text{(A9)}$$

$$S^{(3)}_{\mathrm{NR,rw}} = (\tilde{R}_{1g}) + (\tilde{R}_{4g}) - (\tilde{R}^*_{2f}), \quad \text{(A10)}$$

$$S^{(3)}_{DC,rw} = -(\tilde{R}^*_{3f}) + (\tilde{R}_{4f}). \quad \text{(A11)}$$

APPENDIX B: ORIENTATIONAL AVERAGE

In liquid solution the dimers will not exhibit a preferred orientation, but are oriented isotropically. To perform the orientational averaging of the third-order polarization, it is customary to write the orientationally averaged response functions as

$$\langle (\tilde{R}_n)_{\alpha\beta\gamma\delta}\rangle = \sum_{\nu\kappa\chi\lambda} R_n^{\nu\kappa\chi\lambda} \left\langle \tilde{Y}^{\nu\kappa\chi\lambda}_{\alpha\beta\gamma\delta}\right\rangle, \quad \text{(B1)}$$

with orientation independent response functions $R_n^{\nu\kappa\chi\lambda}$ and functions

$$\left\langle \tilde{Y}^{\nu\kappa\chi\lambda}_{\alpha\beta\gamma\delta}\right\rangle = \langle (\hat{\mu}_\nu)_\alpha (\hat{\mu}_\kappa)_\beta (\hat{\mu}_\chi)_\gamma (\hat{\mu}_\lambda)_\delta\rangle, \quad \text{(B2)}$$

which contain all the information on the orientation.[45,48] Here, as in Eq. (B1), $\langle\cdots\rangle$ denotes the orientational average. Note that in Eq. (B2) only the orientations of the transition dipoles enter (denoted by a hat). Their magnitudes are contained in $R_n^{\nu\kappa\chi\lambda}$. The indices $\{\nu,\kappa,\chi,\lambda\}$ denote the sequences of transitions involved in the calculation of a certain response function $\tilde{R}_n$. For example, for the calculation of $\tilde{R}_1$, $\hat{\mu}_\nu$ can be either $\hat{\mu}_{\mathbf{gb_1}}$ or $\hat{\mu}_{\mathbf{gb_2}}$. As before, for instance the index α denotes the projection of the molecular frame vectors $\hat{\mu}_\nu$ onto the laboratory frame axis α, which is related to the polarization of the laser pulses according to Eq. (15).

If one parametrizes the orientation of the dimer with respect to the laboratory frame, as sketched in Fig. 8, then one has $\left\langle \tilde{Y}_{\alpha\beta\gamma\delta}^{\nu\kappa\chi\lambda}\right\rangle = \int d\phi d\zeta d\psi \sin(\zeta)(\hat{\mu}_\nu)_\alpha(\hat{\mu}_\kappa)_\beta(\hat{\mu}_\chi)_\gamma(\hat{\mu}_\lambda)_\delta P_0$ with the initial isotropic probability $P_0 = \frac{1}{8\pi^2}$. As explained in Sec. II (see Eqs. (11) and (12), together with Eqs. (13) and (14)) the transition dipoles entering in the calculation of the response functions are aligned parallel to either the x- or the y-axis of the molecular frame. Since in the present work we take all electric fields to be linearly polarized in the same direction (which we take as the Z-axis of the laboratory system), we have only to evaluate expressions of the form $\langle a\,b\,c\,d\rangle$ where $\{a, b, c, d\}$ is either $\hat{x}_Z = \sin\zeta$ or $\hat{y}_Z = \cos\zeta$.

The final result for the orientationally averaged response function is given in Appendix B.

For our choice of the polarization direction, not all possible contributions to a response function survive the orientational averaging. For example for $\tilde{R}_1$ from Eq. (A1), one of the excitation sequences which gives no contributions after the averaging is $(\vec{\mu}_{\mathbf{gb_1}})_\alpha(\vec{\mu}_{\mathbf{b_2g}})_\beta(\vec{\mu}_{\mathbf{gb_2}})_\gamma(\vec{\mu}_{\mathbf{b_2g}})_\delta$. However, this kind of terms is equal to zero anyway due to the secular approximation introduced in Sec. V A.

Note that we assume the orientation of the molecular frame of the dimer to remain fixed. Only the relative orientation of the monomers depends on time.

After taking the orientational average under the assumption that all pulses are polarized in $\hat{Z}$-direction, the equations (A1)–(A8) can be reformulated again.

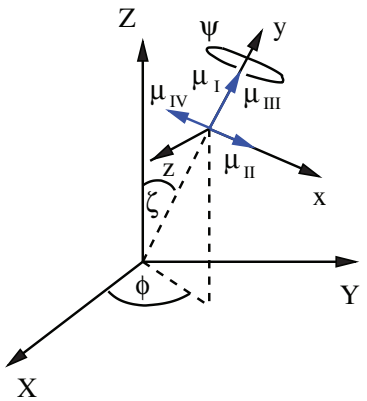

FIG. 8. Sketch of the laboratory frame (axes X, Y, Z) and molecular reference system (axes x, y, z). For the transformation the Euler angles ϕ, ζ, and ψ are used. The transition dipole moments of the dimer μ_I, μ_{II}, μ_{III}, and μ_{IV} are lying in the x-y-plane, see Fig. 1.

$$\mathcal{O}^1_{GSB,ij} = \begin{cases} \frac{1}{5}, & i = j \\ \frac{1}{15}, & i \neq j \end{cases}, \tag{B3}$$

$$\mathcal{O}^1_{DC,ij} = \begin{cases} \frac{1}{5}, & i = j \\ -\frac{1}{15}, & i \neq j \end{cases}, \tag{B4}$$

$$\mathcal{O}^2_{ESE,ij,ch} = \begin{cases} \frac{1}{5}, & i = j = c = h \\ \frac{1}{15}, & \begin{cases} i = c \text{ and } j = h \text{ and } i \neq j \\ i = j \text{ and } c = h \text{ and } i \neq c \\ i = h \text{ and } j = c \text{ and } i \neq j \end{cases} \\ 0, & \text{otherwise} \end{cases} \tag{B5}$$

$$\mathcal{O}^2_{ESA,ij,ch} = \begin{cases} \frac{1}{5}, & i = j = c = h \\ \frac{1}{15}, & i = j \text{ and } c = h \text{ and } i \neq c \\ -\frac{1}{15}, & \begin{cases} i = c \text{ and } j = h \text{ and } i \neq j \\ i = h \text{ and } j = c \text{ and } i \neq j \end{cases} \\ 0, & \text{otherwise} \end{cases}, \tag{B6}$$

$$R_1(\omega_\tau, T, \omega_t) = \sum_{\substack{\{c,h,i,j\} \\ \in\{\mathbf{b_2},\mathbf{b_1}\}}} \mathcal{O}^2_{ESE,ij,ch}\, \mu_{\mathbf{g}i}\mathcal{G}^{(+)}_{i\mathbf{g}}(\omega_t)\,\mu_{\mathbf{g}j} \times \mathcal{G}_{ij,ch}(T)\,\mu_{h\mathbf{g}}\mathcal{G}^{(+)}_{c\mathbf{g}}(\omega_\tau)\,\mu_{c\mathbf{g}}, \tag{B7}$$

$$R_2(\omega_\tau, T, \omega_t) = \sum_{\substack{\{d,g,i,j\} \\ \in\{\mathbf{b_2},\mathbf{b_1}\}}} \mathcal{O}^2_{ESE,ij,gd}\, \mu_{\mathbf{g}i}\mathcal{G}^{(+)}_{i\mathbf{g}}(\omega_t)\,\mu_{\mathbf{g}j} \times \mathcal{G}_{ij,gd}(T)\,\mu_{g\mathbf{g}}\mathcal{G}^{(-)}_{\mathbf{g}d}(\omega_\tau)\,\mu_{d\mathbf{g}}, \tag{B8}$$

$$R_3(\omega_\tau, T, \omega_t) = \sum_{\substack{\{d,k\} \\ \in\{\mathbf{b_2},\mathbf{b_1}\}}} \mathcal{O}^1_{GSB,dk}\mu_{\mathbf{g}k}\mathcal{G}^{(+)}_{k\mathbf{g}}(\omega_t)\,\mu_{k\mathbf{g}} \times \mathcal{G}_{\mathbf{gg}}(T)\,\mu_{\mathbf{g}d}\mathcal{G}^{(-)}_{\mathbf{g}d}(\omega_\tau)\,\mu_{d\mathbf{g}}, \tag{B9}$$

$$R_4(\omega_\tau, T, \omega_t) = \sum_{\substack{\{c,k\} \\ \in\{\mathbf{b_2},\mathbf{b_1}\}}} \mathcal{O}^1_{GSB,ck}\,\mu_{\mathbf{g}k}\mathcal{G}^{(+)}_{k\mathbf{g}}(\omega_t)\,\mu_{k\mathbf{g}} \times \mathcal{G}_{\mathbf{gg}}(T)\,\mu_{\mathbf{g}c}\mathcal{G}^{(+)}_{c\mathbf{g}}(\omega_\tau)\,\mu_{c\mathbf{g}}, \tag{B10}$$

$$R^*_1(\omega_\tau, T, \omega_t) = \sum_{\substack{\{d,g,i,j\} \\ \in\{\mathbf{b_2},\mathbf{b_1}\}}} \mathcal{O}^2_{ESA,ij,gd}\,\mu_{j\mathbf{f}}\mathcal{G}^{(+)}_{\mathbf{f}j}(\omega_t)\,\mu_{\mathbf{f}i} \times \mathcal{G}_{ij,gd}(T)\,\mu_{g\mathbf{g}}\mathcal{G}^{(-)}_{\mathbf{g}d}(\omega_\tau)\,\mu_{d\mathbf{g}}, \tag{B11}$$

$$R^*_2(\omega_\tau, T, \omega_t) = \sum_{\substack{\{c,h,i,j\} \\ \in\{\mathbf{b_2},\mathbf{b_1}\}}} \mathcal{O}^2_{ESA,ij,ch}\,\mu_{j\mathbf{f}}\mathcal{G}^{(+)}_{\mathbf{f}j}(\omega_t)\,\mu_{\mathbf{f}i} \times \mathcal{G}_{ij,ch}(T)\,\mu_{h\mathbf{g}}\mathcal{G}^{(+)}_{c\mathbf{g}}(\omega_\tau)\,\mu_{c\mathbf{g}}, \tag{B12}$$

$$R_3^*(\omega_\tau, T, \omega_t) = \sum_{\substack{\{c,l\} \\ \in\{\mathbf{b_2},\mathbf{b_1}\}}} \mathcal{O}^1_{DC,lc}\, \mu_{l\mathbf{f}} \mathcal{G}^{(+)}_{\mathbf{fl}}(\omega_t)\, \mu_{l\mathbf{g}} \mathcal{G}^{(+)}_{\mathbf{fg}}(\omega_\tau)\, \mu_{\mathbf{f}c} \times \mathcal{G}_{c\mathbf{g}}(T)\, \mu_{c\mathbf{g}} \delta(T), \quad \text{(B13)}$$

$$R_4^*(\omega_\tau, T, \omega_t) = \sum_{\substack{\{d,l\} \\ \in\{\mathbf{b_2},\mathbf{b_1}\}}} \mathcal{O}^1_{DC,ld}\, \mu_{\mathbf{g}l} \mathcal{G}^{(+)}_{l\mathbf{g}}(\omega_t)\, \mu_{l\mathbf{f}} \mathcal{G}^{(+)}_{\mathbf{fg}}(\omega_\tau)\, \mu_{\mathbf{f}d} \times \mathcal{G}_{d\mathbf{g}}(T)\, \mu_{d\mathbf{g}} \delta(T). \quad \text{(B14)}$$

APPENDIX C: DOUBLE COHERENCE CONTRIBUTION

In the response functions R_3^* and R_4^* the factor $\delta(T)$ appears based on the assumption that the pulses are instantaneous and that the time intervals can be approximately considered as being contracted to zero. Accordingly, double coherence contributions can only appear at $T = 0$ fs. Thus, the distinction between different relaxation mechanisms plays no role for double coherence contributions.

[1] R. E. Merrifield, Radiat. Res. **20**, 154 (1963).
[2] R. Fulton and M. Gouterman, J. Chem. Phys. **41**, 2280 (1964).
[3] T. Förster, in *Modern Quantum Chemistry III*, edited by O. Sinanoglu (Academic, New York, 1965).
[4] J. Seibt, P. Marquetand, V. Engel, Z. Chen, V. Dehm, and F. Würthner, Chem. Phys. **328**, 354 (2006).
[5] A. Eisfeld, Chem. Phys. Lett. **445**, 321 (2007).
[6] M. H. Hennessy, Z. G. Soos, R. A. Pascal, and A. Girlando, Chem. Phys. **245**, 199 (1999).
[7] A. Eisfeld, L. Braun, W. Strunz, J. Briggs, J. Beck, and V. Engel, J. Chem. Phys. **122**, 134103 (2005).
[8] J. Guthmuller, F. Zutterman, and B. Champagne, J. Chem. Theory Comput. **4**, 2094 (2008).
[9] J. Guthmuller, F. Zutterman, and B. Champagne, J. Chem. Phys. **131**, 154302 (2009).
[10] J. Roden, A. Eisfeld, M. Dvořák, O. Buenermann, and F. Stienkemeier, J. Chem. Phys. **134**, 054907 (2011).
[11] C. G. Heid, P. Ottiger, R. Leist, and S. Leutwyler, J. Chem. Phys. **135**, 154311 (2011).
[12] M. Kasha, Radiat. Res. **20**, 55 (1963).
[13] M. Kasha, H. R. Rawls, and M. Ashraf El-Bayoumi, Pure Appl. Chem. **2**, 371 (1965).
[14] R. F. Fink, J. Seibt, V. Engel, M. Renz, M. Kaupp, S. Lochbrunner, H.-M. Zhao, J. Pfister, F. Würthner, and B. Engels, J. Am. Chem. Soc. **130**, 12858 (2008).
[15] W. Liu, V. Settels, P. H. P. Harbach, A. Dreuw, R. F. Fink, and B. Engels, J. Comput. Chem. **32**, 1971 (2011).
[16] M. Cho, Chem. Rev. **108**, 1331 (2008).
[17] A. Schubert and V. Engel, J. Chem. Phys. **134**, 104304 (2011).
[18] D. Abramavicius, B. Palmieri, D. V. Voronine, F. Šanda, and S. Mukamel, Chem. Rev. **109**, 2350 (2009).
[19] T. Brixner, J. Stenger, H. M. Vaswani, M. Cho, R. E. Blankenship, and G. R. Fleming, Nature (London) **434**, 625 (2005).
[20] N. S. Ginsberg, Y.-C. Cheng, and G. R. Fleming, Acc. Chem. Res. **42**, 1352 (2009).
[21] L. Z. Sharp, D. Egorova, and W. Domcke, J. Chem. Phys. **132**, 014501 (2010).
[22] L. Yang, D. Abramavicius, and S. Mukamel, New J. Phys. **12**, 065046 (2010).
[23] D. Hayes, G. Panitchayangkoon, K. A. Fransted, J. R. Caram, J. Wen, K. F. Freed, and G. S. Engel, New J. Phys. **12**, 065042 (2010).
[24] D. Hayes and G. Engel, Biophys. J. **100**, 2043 (2011).
[25] A. G. Dijkstra, T. L. C. Jansen, and J. Knoester, J. Chem. Phys. **128**, 164511 (2008).
[26] F. Milota, J. Sperling, A. Nemeth, and H. Kauffmann, Chem. Phys. **357**, 45 (2009).
[27] L. Chen, R. Zheng, Q. Shi, and Y. Yan, J. Chem. Phys. **132**, 024505 (2010).
[28] P. Kjellberg, B. Brüggemann, and T. Pullerits, Phys. Rev. B **74**, 024303 (2006).
[29] T. Mančal and G. Fleming, J. Chem. Phys. **121**, 10556 (2004).
[30] A. V. Pisliakov, T. Mančal, and G. R. Fleming, J. Chem. Phys. **124**, 234505 (2006).
[31] V. Szöcs, T. Pálszegi, V. Lukeš, J. Sperling, F. Milota, W. Jakubetz, and H. Kauffmann, J. Chem. Phys. **124**, 124511 (2006).
[32] A. Moran, J. Maddox, J. Hong, J. Kim, R. Nome, G. Bazan, S. Mukamel, and N. Scherer, J. Chem. Phys. **124**, 194904 (2006).
[33] J. M. Womick and A. M. Moran, J. Phys. Chem. B **113**, 15771 (2009).
[34] G. A. Lott, A. Perdomo-Ortiz, J. K. Utterback, J. R. Widom, A. Aspuru-Guzik, and A. H. Marcus, Proc. Natl. Acad. Sci. U.S.A. **108**, 16521 (2011).
[35] D. M. Jonas, Annu. Rev. Phys. Chem. **54**, 425 (2003).
[36] M. Topaler, T. Allison, D. Schwenke, and D. Truhlar, J. Chem. Phys. **109**, 3321 (1998).
[37] V. May and O. Kühn, *Charge and Energy Transfer Dynamics in Molecular Systems* (Wiley VCH, Berlin, 2004).
[38] A. Nemeth, F. Milota, T. Mančal, T. Pullerits, J. Sperling, J. Hauer, H. F. Kauffmann, and N. Christensson, J. Chem. Phys. **133**, 094505 (2010).
[39] J. M. Jean and G. R. Fleming, J. Chem. Phys. **103**, 2092 (1995).
[40] M. Wewer and F. Stienkemeier, Phys. Rev. B **67**, 125201 (2003).
[41] P. F. Tekavec, G. A. Lott, and A. H. Marcus, J. Chem. Phys. **127**, 214307 (2007).
[42] D. Abramavicius, D. V. Voronine, and S. Mukamel, Biophys. J. **94**, 3613 (2008).
[43] E. L. Read, G. S. Engel, T. R. Calhoun, T. Mancăl, T. K. Ahn, R. E. Blankenship, and G. R. Fleming, Proc. Natl. Acad. Sci. U.S.A. **104**, 14203 (2007).
[44] J. Dreyer, A. Moran, and S. Mukamel, Bull. Korean Chem. Soc. **24**, 1091 (2003).
[45] R. M. Hochstrasser, Chem. Phys. **266**, 273 (2001).
[46] O. Roslyak, C. A. Marx, and S. Mukamel, Phys. Rev. A **79**, 033832 (2009).
[47] T. Brixner, T. Mančal, I. V. Stiopkin, and G. R. Fleming, J. Chem. Phys. **121**, 4221 (2004).
[48] O. Golonzka and A. Tokmakoff, J. Chem. Phys. **115**, 297 (2001).
[49] This value is obtained from the curvature of the ground-state potential around the minimum and the quantum chemical result for the lowest eigenfrequency of the torsional motion, which was calculated with the dispersion corrected density functional (DFT-D1) theory [R. Fink, private communication (2011)]. The resulting moment of inertia is in rough agreement with the torsional constant obtained from the molecular geometry $\sim 1.063 \times 10^{-43}$ kg m^2.
[50] We assume δ-shaped Laser pulses.